



Influence of atmospheric deposition on biogeochemical cycles in an oligotrophic ocean system

France Van Wambeke¹, Vincent Taillandier², Karine Desboeufs³, Elvira Pulido-Villena¹, Julie Dinasquet^{4,5}, Anja Engel⁶, Emilio Marañón⁷, Céline Ridame⁸, Cécile Guieu²

5

¹ Aix-Marseille Université, CNRS/INSU, Université de Toulon, IRD, Mediterranean Institute of Oceanography (MIO) UM 110, 13288, Marseille, France

² CNRS, Sorbonne Université, Laboratoire d'Océanographie de Villefranche (LOV), UMR7093, 06230 Villefranche-sur-Mer, France

10 ³ LISA, UMR CNRS 7583, Université Paris-Est-Créteil, Université de Paris, Institut Pierre Simon Laplace (IPSL), Créteil, France

⁴ Sorbonne Universités, Laboratoire d'Océanographie Microbienne (LOMIC), Observatoire Océanologique, 66650, Banyuls/mer

⁵ Marine Biology Research Division, Scripps Institution of Oceanography, UCSD, La Jolla, USA

15 ⁶ GEOMAR – Helmholtz-Centre for Ocean Research, Kiel, Germany

⁷ Department of Ecology and Animal Biology, Universidade de Vigo, 36310 Vigo, Spain

⁸ Sorbonne University/CNRS/IRD/MNHN, LOCEAN: Laboratoire d'Océanographie et du Climat: Expérimentation et Approches Numériques, UMR 7159, 4 Place Jussieu – 75252 Paris Cedex 05, France

Correspondence to: France Van Wambeke (france.van-wambeke@mio.osupytheas.fr) and
20 Cécile Guieu (guieu@obs-vlfr.fr)

Abstract.

The surface mixed layer (ML) in the Mediterranean Sea is a well stratified domain characterized by low macro-nutrient and low chlorophyll content, during almost 6 months of the year. Nutrient dynamics in the ML depend on allochthonous inputs, through atmospheric deposition and on biological recycling. Here we characterize the biogeochemical cycling of N in the ML by combining simultaneous *in situ* measurements of atmospheric deposition, nutrients, hydrological conditions, primary production, heterotrophic prokaryotic production, N₂ fixation and leucine aminopeptidase activity. The measurements were conducted along a 4300 km transect across the central and western open Mediterranean Sea in spring 2017. Dry deposition was measured on a continuous basis while two wet deposition events were sampled, one in the Ionian Sea and one in the Algerian basin. Along the transect, N budgets were computed to compare sources and sinks of N in the mixed layer. On average,



phytoplankton N demand was 2.9 fold higher (range 1.5-8.1) than heterotrophic prokaryotic N demand. *In situ* leucine aminopeptidase activity contributed from 14 to 66 % of heterotrophic prokaryotic N demand, and N₂ fixation rate represented 1 to 4.5 % of the phytoplankton N demand. Dry atmospheric deposition of inorganic nitrogen, estimated from dry deposition of (nitrate+ammonium) in aerosols, was higher than N₂ fixation rates in the ML (on average 4.8 fold). The dry atmospheric input of inorganic N represented a highly variable proportion of biological N demand in the ML, 10-82% for heterotrophic prokaryotes and 1-30% for phytoplankton. Stations visited for several days allowed following the evolution of biogeochemical properties in the ML and within the nutrient depleted layers. At the site in the Algerian Basin and on a basis of high frequency sampling of CTD casts before and after a wet dust deposition event, different scenarios were considered to explain a delayed appearance of peaks in dissolved inorganic phosphate in comparison to nitrate within the ML. After the rain, nitrate was higher in the ML than in the nutrient depleted layer below. Estimates of nutrient transfer from the ML to the nutrient depleted layer could explain $\frac{1}{3}$ of the nitrate fate out of the ML. Luxury consumption of P by heterotrophic prokaryotes, further transferred in the microbial food web, and remineralized by grazers, is one explanation for the delayed phosphate peak of DIP. The second explanation is a transfer from ML to the nutrient depleted layer below through adsorption/desorption processes on particles. Phytoplankton did not benefit directly from atmospheric inputs in the ML, probably due to a high competition with heterotrophic prokaryotes, also limited by N and P availability at the time of this study. Primary producers, in competition for nutrients with heterotrophic prokaryotes, decreased their production after the rain, recovering their initial state of activity after 2 days lag in the vicinity of the deep chlorophyll maximum layer.

1. Introduction

The Mediterranean Sea (MS) is a semi-enclosed basin characterized by very short ventilation and residence times with respect to its own thermohaline circulation (Mermex Group, 2011). In terms of biogeochemistry, MS is characterized by a long summer stratification period. It is a low nutrient, low chlorophyll (LNLC) system with a general west-to-east gradient of increasing oligotrophy, and an overall phosphorus (P) deficit compared to nitrogen (N) (Mermex Group, 2011). This is evidenced by higher N/P than Redfield ratios of inorganic nutrients in deep layers, increasing to the east (Krom et al., 2010).



65 The nature of the relationship between photoautotrophic unicellular organisms and heterotrophic prokaryotes (competition or commensalism) is affected by the balance of light and nutrients experienced by phytoplankton as well as possible inputs of organic matter from river runoff or atmospheric deposition. Phytoplankton generally experience P, N, or NP limitations (Thingstad et al., 2005 ; Tanaka et al., 2011, Richon et al., 2018), whereas

70 heterotrophic prokaryotes are usually P or P+labile carbon co-limited (Sala et al., 2002, Van Wambeke et al., 2002, Céa et al., 2014).

The MS continuously receives anthropogenic aerosols originating from industrial and domestic activities from all around the basin and other parts of Europe and pulsed natural inputs from the Sahara. It is thus, a natural LNLC laboratory well adapted to explore the role

75 of ocean–atmosphere exchanges of particles and gases on marine biogeochemical cycles.

Parameterization and representation of the key processes brought into play by atmospheric deposition in MS must take into account the role of pulsed atmospheric inputs (Guieu et al., 2014a). Recent studies describe annual records of atmospheric deposition of trace metals and inorganic macronutrients (N, P) obtained in several atmospheric stations located around the

80 MS (Markaki et al., 2010; Guieu and Ridame, in press; Desboeufs, in press). All records denote the pulsed and highly variable inputs. Recent models and observations show that atmospheric deposition of organic matter (OM) is also highly variable and that annual atmospheric inputs of OM are of the same order of magnitude as river inputs (Djaoudi et al., 2017, Kanakidou et al., 2018; Kanakidou et al., 2020). Moreover, the sum of atmospheric

85 inputs of nitrate, ammonium and soluble organic nitrogen has been shown to be equivalent or higher than those of N₂ fixation rates (Sandroni et al., 2007), although inorganic atmospheric N inputs alone might also be higher than N₂ fixation rates (Bonnet et al., 2011).

Aerosol amendments in bottles, minicosms, or mesocosms have been widely used to study trophic transfer and potential export, as they represent to some extent a ‘simplified’ plankton

90 trophic web studied in the vertical dimension (i.e. Guieu et al. 2010; Herut et al., 2016). Both diversity and functioning of various biological compartments have been shown to be impacted by aerosol additions in different tested waters of the Mediterranean Sea (Guieu and Ridame, in press, and synthesis Figure 3 therein). Differences in the biological responses have been observed, depending on the mode of deposition (wet or dry) mimicked, the type of aerosols

95 (natural or anthropogenic) used and the *in situ* biogeochemical conditions at the time of the experiment (Guieu and Ridame, in press).



Organic carbon from aerosols is partly soluble, and this soluble fraction is partly available to marine heterotrophic prokaryotes (Djaoudi et al., 2020). Heterotrophic prokaryotes have the metabolic ~~capacities~~ to respond quickly to aerosol deposition through growth and changes in 100 community composition (Rahav et al., 2016; Pulido-Villena et al., 2008; 2014), while the phytoplankton community respond~~s~~ slower or not at all (Guieu and Ridame, in press, and reference therein).

Owing to the intrinsic limitations, which vary depending on the size and design of enclosures, 105 i.e. without the representation of higher trophic levels, in absence of turbulent mixing that limited exchanges to diffusion, wall effects~~s~~; such experiments cannot fully simulate *in situ* conditions (Guieu and Ridame, in press). Thus, it is still necessary to acquire *in situ* observations of the ~~the consequences~~ of aerosol deposition on biogeochemical cycles.

However, *in situ* studies of aerosol deposition are scarce and require high frequency sampling 110 to follow the effects of deposition on biogeochemical processes. For instance, the biological response to a Saharan dust event of 2.6 g m^{-2} recorded at a land station (Cap Ferrat) was detected 4 days after by only one water column sampling offshore (at DYFAMED observation site), and analysis showed increases in heterotrophic prokaryotic respiration and 115 abundances by comparison to a sampling date done 16 days before this dust event (Pulido-Villena et al., 2008). In the Israeli coast, a moderate natural dust storm (1.05 mg L^{-1} over 5 m depth) was followed every 12 h during 5 days (Rahav et al., 2016). These authors observed rapid changes which may have been missed without high frequency sampling. They reported 120 a decrease in picophytoplankton abundance, an increase in heterotrophic prokaryotes abundance, as well as~~s~~ slight increase in primary production (25%) and heterotrophic prokaryotic production (15%).

Hence, it is necessary to organize sampling surveys with adaptative strategies to follow 125 aerosol deposition events *in situ* and their impacts on biogeochemical processes, especially in the open waters of the summer stratified and nutrient limited MS. The objectives of the PEACETIME project were to study fundamental processes and their interactions at the ocean–atmosphere interface after atmospheric deposition (especially of Saharan dust) in the Mediterranean Sea, and how these processes impact the functioning of the pelagic ecosystem (Guieu et al., 2020).

As atmospheric deposition affects primarily the surface mixed layer (ML), the present study focuses on the upper part of the nutrient depleted layer that extends down to the nutriclines (as defined by Du et al., 2017). During the stratification period, the concentrations of nitrate and



130 phosphate within the ML are often below quantification limits of standard methods. However, nanomolar concentrations of nitrate (and phosphate) can now be assessed accurately through Long Waveguide Capillary Cell (LWCC) technique, which allows to measure fine gradients inside nutrient depleted layers in the MS (Djaoudi et al., 2018).

135 The aims of the present study were to assess the impact of atmospheric nutrient deposition on biogeochemical processes and fluxes in the open sea during a cruise in the MS. For this i) we estimated nanomolar variations of nitrate concentration in the surface mixed layer (ML) facing variable inputs of dry and wet aerosols deposition ii) we compared the aerosols-derived N inputs to the ML with biological activities: primary production, heterotrophic prokaryotic production, N₂ fixation and ectoenzymatic activity (leucine aminopeptidase). We studied

140 these N budgets along a 13 stations transect crossing the Algerian Basin, Tyrrhenian Sea and the Ionian Sea where dry atmospheric deposition was continuously measured on board together with seawater biogeochemical and biological characteristics. We finally focused on a high frequency sampling of a wet deposition event that occurred in the western Algerian Basin, during which we investigated the evolution of biogeochemical fluxes of both N and P

145 and microbial activities.

2. Materials and Methods

2.1 Sampling strategy and measured parameters

150 The PEACETIME cruise (doi.org/10.17600/15000900) was conducted in the Mediterranean Sea, from May to June 2017, along a transect extending from the Western Basin to the center of the Ionian Sea (Fig. 1). For details on the cruise strategy, see Guieu et al. (2020). Short duration stations (< 8 h, 15 stations named ST1 to ST10, Fig. 1) and long duration sites (5 days, 3 sites named TYR, ION and FAST) were occupied. Chemical composition of aerosols was quantified by continuous sampling along the whole transect. In addition, two rain events 155 were sampled (Fu et al., this issue, in prep. b), one on the 29th of May at ION station, and a second one, a dust wet deposition event, at FAST site on the 5th of June.

At least 3 CTD casts were conducted at each short station. One focused on the epipelagic layer (0-250 m), and the second one on the whole water column. Both were sampled with a standard, classical-CTD rosette equipped with a sampling system of 24 Niskin bottles (12 L), 160 and a Sea-Bird SBE9 underwater unit equipped with pressure, temperature (SBE3), conductivity (SBE4), chlorophyll fluorescence (Chelsea Aquatracka) and oxygen (SBE43) sensors. The third cast, from surface to bottom was performed under ‘trace metal clean



conditions' using a second instrumental package including a titanium rosette (called TMC-rosette) mounted on a Kevlar cable and equipped with Go-Flo bottles that were sampled in a
165 dedicated clean lab container. The long sites were abbreviated as TYR (situated in the center of the Tyrrhenian Basin), ION (in the center of the Ionian Basin), FAST (in the western Algerian Basin). These 3 sites were selected using satellite imagery, altimetry and Lagrangian diagnostics and forecasted events of rain (Guieu et al., 2020). At these sites, repeated casts were performed during at least 5 days, alternating CTD- and TMC- rosettes. TYR site was
170 occupied from May 17, 05:08 to May 21, 15:59 and ION site from May 24, 18:02 to May 29, 8:25. FAST site was occupied from June 2, 20:24 to June 7, 23:25 and then from June 8, 21:06 to June 9, 00:16 (all times in local time). The succession of CTD casts at FAST site are numbered in days relative to a rain event collected on board the ship that ended on June 5, 3:04. The first cast of the series was sampled 2.3 days before that rain, and the last one 2 days
175 after. The FAST site was occupied a second time after the study of ST10 (3.8 days after the rain event).

Primary production (PP), prokaryotic heterotrophic production (BP), heterotrophic prokaryotic abundances (hprok), ectoenzymatic activities (leucine aminopeptidase (LAP) and alkaline phosphatase (AP)), were determined on water samples collected with the classical
180 CTD-rosette. Inorganic nutrients, dissolved organic nitrogen (DON) and phosphorus (DOP) were measured on water samples collected by the TMC-rosette. LAP and AP were determined on two layers in the epipelagic waters (5 m depth and deep chlorophyll maximum (DCM)) at the short stations as well as at ION and TYR stations. In addition, for 4 profiles at FAST, LAP and AP were determined at 4 depths between 0 and 20 m to get insight on the variability
185 within the ML.

2.2 Analytical methods and fluxes calculations

2.2.1 Nutrients in the atmosphere

Description of the atmospheric deposition strategy is detailed in Desboeufs et al. (this issue, in
190 prep). In summary, the total suspended aerosol particles (TSP inlet) were continuously collected during the campaign, either by filtration units on adapted membranes for off-line chemical analysis or by aerosol water extraction unit, a Particle-into-Liquid-Sampler (PILS, Orsini et al., 2003), for on-line analyses of major water soluble ions. Moreover, two wet deposition events were sampled on board the ship during the cruise (details in Fu et al., this
195 issue, in prep. b), one at ION site, one at FAST site. At FAST, casts were performed before,



and after the rain event at a high frequency with a fine definition of the sampling within the mixed layer, between surface and 20 m depth. This was done also at ION but with a lower frequency. Also, a strong dust deposition event, with intense wet deposition, likely occurred over the Tyrrhenian Sea around May 11-12th, a few days before our arrival on site

200 (Desboeufs et al., this issue, in prep.). Using particulate aluminum inventory in the water column, the dust deposition was estimated to be 5.5-5.9 g m⁻² at ST5, 0.8-1.6 at TYR and 1.6-1.9 at ST6 (Bressac et al., this issue, in prep.).

Nitrate and ammonium concentrations in aerosols, abbreviated in the text as NO₃ and NH₄, respectively, (nitrite concentrations were under analytical detection limits) were continuously

205 analyzed on board from May 13 by PILS sampling coupled on-line with a double way ion chromatography (PILS-IC, Metrohm, model 850 Professional IC with Metrosep A Supp 7 column for anions measurements and Metrosep C4 column for cation measurements; Fu et al., this issue, in prep a). Inorganic phosphate (DIP) concentrations were estimated from total phosphorus concentrations in particulate aerosols on filters since it was generally under

210 detection limits using the PILS-IC technique. NO₃, NH₄ and DIP were also determined by ion chromatography in the dissolved fraction of the 2 rain samples.

Atmospheric dry deposition fluxes of inorganic nitrogen were estimated by multiplying the aerosol concentrations of NO₃ and NH₄ by the dry settling velocities of N-bearing aerosols, i.e. 0.21 and 1 cm s⁻¹ for NH₄ and NO₃, respectively (Kouvarakis et al., 2001). The

215 concentrations used were averages from PILS-IC analysis obtained during the occupation of each short station, and averages between two successive casts during site occupations, except for ST1 where concentrations were issued from filter by IC analyses after water extraction. This period lasted from 0.13 to 0.66 days for short stations and from 0.41 to 1.21 days for sites. Atmospheric dry deposition of inorganic P was estimated using the total P particulate

220 aerosol concentration multiplied by a dry settling velocity of 1 cm s⁻¹ except 3 cm s⁻¹ at FAST site, as this value is more adapted for Saharan events (Izquierdo et al., 2012), hence this value is likely an upper range for DIP. At each short station, total P was determined from the filter sampled during the period of the short station and this period of filter collection ranged 0.28 - 1.15 days according to the stations. At the 3 sites, we used filters collecting aerosols during

225 periods including the CTD casts sampling date, when possible. The wet deposition fluxes were estimated from the measured concentrations in the filtrate phase of rain (0.2 μm), the rain volume and the surface of the rain funnel (Fu et al., this issue, in prep. b).



2.2.2 Nutrients in the water column

230 Seawater samples for standard dissolved nutrient analysis were filtered online (< 0.2 µm, Sartorius Sartobran-P-capsule with a 0.45 µm prefilter and a 0.2 µm final filter) directly from the GoFLo bottles (TMC-rosette). Samples collected in acid-washed polyethylene bottles were immediately analyzed on board. Micromolar nitrate + nitrite (NO_x) and DIP were determined using a segmented flow analyzer (AAIII HR SealAnalytical©) following Aminot and Kérouel (2007) with a limit of quantification of 0.050 µM for NO_x and 0.020 µM for DIP. Samples for the determination of nanomolar concentrations of dissolved nutrients were collected in HDPE bottles previously cleaned with supra-pure HCl. For NO_x (considered as NO₃ as nitrite fraction was mostly negligible), samples were acidified to pH 1 inside the clean van and analyzed back to the laboratory using a spectrometric method in the visible at 540 nm, with a 1 m LWCC (Louis et al., 2015). The limit of detection was 6 nM, the limit of quantification was 9 nM and the reproducibility was 8.5%. DIP was analyzed immediately after sampling using the LWCC method after Pulido-Villena et al. (2010), with a limit of detection of 1 nM. Total dissolved phosphorus (TDP) and nitrogen (TDN) were measured using the segmented flow analyzer technique after high-temperature (120 °C) persulfate wet oxidation mineralization (Pujo-Pay and Raimbault, 1994). DOP (DON) was obtained as the difference between TDP (TDN) and DIP (NO_x). Labile DOP (L-DOP) was determined as 31% DOP (Pulido-Villena et al., this issue, in prep.).

240 Total hydrolysable amino acids (TAA) were determined as described in detail in Van Wambeke et al. (2020). Briefly 1 ml of sample were hydrolyzed at 100°C for 20 h with 1 ml of 30% HCl and then neutralized by acid evaporation. Samples were analyzed by high performance liquid chromatography according to Dittmar et al. (2009) protocols.

250

2.2.3 Biological stocks and fluxes in the epipelagic waters

For the enumeration of autotrophic prokaryotic and eukaryotic cells, heterotrophic prokaryotes (hprok) and heterotrophic nanoflagellates (HNF) by flow cytometry, subsamples (4.5 mL) were fixed with glutaraldehyde grade I 25% (1% final concentration), flash frozen and stored at -80 °C until analysis. Counts were performed on a FACSCanto II flow cytometer (Becton Dickinson). The separation of different autotrophic populations was based on their scattering and fluorescence signals according to Marie et al. (2000). For the enumeration of hprok (Gasol and Del Giorgio, 2000), cells were stained with SYBR Green I

260



(Invitrogen – Molecular Probes). HNF staining was performed with SYBR Green I as described in Christaki et al. (2011). All cell abundances were determined from the flow rate, which was calculated with TruCount beads (BD biosciences).

Particulate primary production (PP) was determined on 6 layers from the shallow (0-250 m) 265 casts sampled before sun rise. Samples were inoculated with ^{14}C -bicarbonate and incubated in on-deck incubators refrigerated with running surface seawater and equipped with various blue screens to simulate different irradiance levels. After incubations during 24 h, samples were filtered through 0.2 polycarbonate filters and treated for liquid scintillation measurement as described in detail in Marañón et al. (2020). A temperature correction was applied as 270 explained in Marañón et al. (2020). N_2 fixation rates (N2fix) were determined as described in Ridame et al. (this issue, in prep) using 2.3 L of unfiltered seawater (acid-washed polycarbonate bottles) enriched with $^{15}\text{N}_2$ gas (99 atom% ^{15}N) to obtain a final enrichment of about 10 atom% excess. Incubations for N2fix were conducted under the same temperature and irradiance as the corresponding PP incubations.

275 To calculate prokaryotic heterotrophic prokaryotic production (BP) epipelagic layers (0-250 m) were incubated with tritiated leucine using the microcentrifuge technique as detailed in Van Wambeke et al. (2020). We used the empirical conversion factor of 1.5 ng C per pmol of incorporated leucine according to Kirchman (1993). Indeed, isotope dilution was negligible under these saturating concentrations as checked occasionally with concentration kinetics. As 280 we used only 2 temperature controlled dark-incubators on board, a temperature correction was applied as explained in Van Wambeke et al. (2020). Ectoenzymatic activities were measured fluorometrically, using fluorogenic model substrates that were L-leucine-7-amido-4-methylcoumarin (Leu-MCA) and 4 methylumbelliferyl – phosphate (MUF-P) to track aminopeptidase activity (LAP), and alkaline phosphatase activity (AP), respectively, are 285 described in details in Van Wambeke et al. (2020). Briefly the release of MCA from Leu-MCA and MUF from MUF-P were followed by measuring increase of fluorescence in the dark (exc/em 380/440 nm for MCA and 365/450 nm for MUF, wavelength width 5 nm) in a VARIOSCAN LUX microplate reader. Fluorogenic substrates were added at varying concentrations in 2 ml wells (0.025, 0.05, 0.1, 0.25, 0.5 and 1 μM) in duplicate. From varying 290 velocities obtained, we determined the parameters V_{\max} (maximum hydrolysis velocity) and K_m (Michaelis-Menten constant that reflects enzyme affinity for the substrate) by fitting the data using a non-linear regression on the following equation:



$$V = V_{max} \times S / (K_m + S)$$

where V is the hydrolysis rate and S the fluorogenic substrate concentration added. TAA and
295 L-DOP were used as substrates to determine LAP and AP *in situ* activities from Michaelis-
Menten equations (Van Wambeke et al., 2020, Pulido-Villena et al, this issue, in prep.).

2.3 Enrichment experiments

At the three long duration sites, enrichment experiments were performed using seawater from
300 5 m depth to assess factors limiting BP in the surface mixed layer. The date of sampling for
these experiments [FAST (June 2, 22:00), TYR (May 16, 20:00) and ION (May 25, 20:00)]
was before the rain event occurring at FAST and at ION. Eight series of triplicate 60 mL
polycarbonate bottles were filled with unfiltered seawater and amended as follows: C : no
enrichment, N: +1 μ M NO₃ + 1 μ M NH₄; P: + 0.2 μ M DIP; G: + 10 μ M C-glucose; NP: N +
305 P; NG : N + G; PG : P + G; NPG: N + P + G. After 48 h incubation in the dark at *in situ*
temperature, BP was determined in the 24 bottles (as described in previous section).

2.4. Vertical partition of the epipelagic layer

The ML can be in a state of stirring and the density and seawater properties are homogeneous,
310 or in a state of rest with homogeneous density but vertical variations of the non-conservative
components (such as nutrients); depending on momentum and heat fluxes at the interface with
the atmosphere that determine the strength and vertical extent of mixing (Brainerd and Gregg,
1995). In the present study, the mixed layer depth (MLD) was estimated indirectly using the
shape of CTD profiles, in absence of concomitant turbulence measurements. Classical
315 methods to evaluate MLD from CTD profiles are based on thresholds of vertical density gap
(de Boyer Montegut et al., 2004; D'Ortenzio et al., 2005) or on the vertical extension of a
fixed buoyancy content (Moutin and Prieur, 2012). As discussed in Gardner et al. (1995), the
choice of criterion is sensitive to discriminate the subtle changes from active mixing to rest,
with consequences in the representative time scales of MLD estimates. In the present study,
320 the ML ~~were~~ shallow (10 - 20 m), rapidly activated by mechanical effects of wind, and
sampled at high frequency (some hours at long duration stations). An approach based on
buoyancy criterion has been preferred to better resolve short term fluctuations in the mixing
state, and MLD was determined as the depth where the residual mass content is equal to 1 kg
 m^{-2} , with an error of estimation of 0.5 m relative to the vertical resolution of the profile (1 m).



325 In the present case of shallow ML in LNLC systems, the nutrient depleted layer comprises the ML and a layer below, referred hereafter as 'NDLb' (b for bottom or base) when examining NO₃ distribution and PDLb when considering DIP distributions. This layer vertically extends between the MLD and the nitracline (phosphacline) depth (Fig. 2). The latter interface is estimated by the depth of the NO₃ (DIP) depletion density, which is the deepest isopycnal at 330 which micromolar NO₃ (DIP) concentration is zero (Kamykowsky and Zentara, 1986; Ormand and Mahadevan, 2015). The NO₃ (DIP) depletion density is estimated at every discrete profile of micromolar NO₃ (DIP) concentrations by the intercept of the regression line reported in a nutrient-density diagram.

335 There are various mechanisms, dynamical or biological, that can trigger exchanges of nutrients between the ML and NDLb (PDLb). Under the hypothesis of vertical (one-dimensional) regimes, the processes of exchange are twice, by diffusion or advection (e.g. Du et al., 2017). The flux of nutrient can be expressed as:

$$F_{NO_3} = F_{DIF} + F_{ADV}$$

340 The diffusive flux F_{DIF} is expressed by the gradient of nutrient concentration times a vertical diffusivity coefficient K_z as:

$$F_{DIF} = K_z \cdot (NO_3_{ML} - NO_3_{NDLb}) / MLD$$

The typical magnitude of K_z in the surface layers of the PEACETIME stations is assessed to $10^{-5} \text{ m}^2 \text{ s}^{-1}$, as discussed in Taillandier et al. (2020).

345 The advective flux F_{ADV} is expressed by the variation of nutrient concentration across the ML times a temporal variation of MLD, as:

$$F_{ADV} = (NO_3_{ML} - NO_3_{NDLb}) \cdot dMLD / dt$$

With shallow ML (10 - 20 m) primarily influenced by wind bursts that lead to intermittent MLD variations of some meters per day (10^{-5} m s^{-1}), the advective fluxes provide transient exchanges of one order of magnitude larger than well-established diffusive fluxes. In 350 consequence, at the time scale of a rain event and the associated rapid variations of MLD, the atmospheric input of nutrients is preferentially exported below the ML by advection rather than by diffusion. In other terms, under the hypothesis of non-stationary regimes due to rapid changes in atmospheric conditions (that control both mixing state of the interface and aerosol nutrient inputs) we assume that vertical advection is the main process of exchange.

355 At short stations and long duration sites, the term $NO_3_{ML} - NO_3_{NDLb}$ can be inferred by difference of nanomolar (LWCC) concentrations inside NDLb relative to the ones inside ML. Since advective flux estimates require the evolution of MLD, they are only accessible at the



long duration sites. At short stations, and in absence of characterization of advective fluxes, only a qualitative assessment of nutrient fluxes across ML can be drawn. When $\text{NO}_3_{\text{ML}} - \text{NO}_3_{\text{NDLb}} < 0$, the NDLb is supplied in nutrients across the nutricline, and then possibly transferred inside the ML, meaning that ML nutrients are impacted by inputs from below. When $\text{NO}_3_{\text{ML}} - \text{NO}_3_{\text{NDLb}} > 0$, the ML is supplied in nutrients from above and exported into the NDLb. Vertical distributions of DIP, along the longitudinal transect, are described in detail in a companion paper (Pulido-Villena et al., this issue, in prep.). In this study, we will focus on phosphate exchanges between ML and PDLb layers at the high-frequency sampled FAST site and relationships with NO_3 distribution.

2.5 Budget from the metabolic fluxes

Trapezoidal integration was used to integrate BP, PP and N₂fix within the ML. The biological activity at surface was considered equal to that of the first layer sampled (around 5 m depth at the short stations, 1 m depth at the FAST site). When the MLD was not sampled, the volumetric activity at this depth was linearly interpolated between 2 closest data above and below the MLD.

We used an approach similar to Hoppe et al. (1993) to compute *in situ* hydrolysis rates for LAP and AP. We assumed that total amino acids (TAA) could be representative of dissolved proteins. *In situ* hydrolysis rates of LAP and AP were determined using molar concentrations of TAA and L-DOP, respectively used as substrate concentration in the Michaelis-Menten kinetics. For LAP, the transformation of *in situ* rates expressed in nmol TAA hydrolysed L⁻¹ h⁻¹ were then transformed in nitrogen units using N per mole TAA, as the molar distributions of TAA were available. Integrated *in situ* LAP hydrolysis rates were calculated assuming the Michaelis-Menten parameters V_m and K_m obtained at 5 m depth to be representative of the whole ML, and thus an average *in situ* volumetric LAP flux in ML was obtained by combining average TAA concentrations in the ML with these kinetic parameters, and then this volumetric rate was simply multiplied by the MLD. Daily BP, AP and LAP integrated activities were calculated from hourly rates x 24. Assuming no direct excretion of either nitrogen or phosphorus, the quota C/N and C/P of cell demand is equivalent to cell biomass quotas. We used C/N ratios derived from Moreno and Martiny, 2018 (range 6-8, mean 7) for phytoplankton and from Nagata et al. (1986) for heterotrophic prokaryotes (range 6.2-8.4, mean 7.1). C/P of sorted cells (cyanobacteria, picophytoeukaryotes) in P depleted conditions



390 ranged 107 to 161 (Martiny et al., 2013), and we considered a mean of 130 for phytoplankton.
A value of 100 was used for heterotrophic prokaryotes (Godwin and Cotner, 2015).

3. Results

395 3.1 Nutrients pattern and biological fluxes along the PEACETIME transect

The ML occupied the first 20 m with an excursion between 9 m in the Ionian Sea (ION site) and 21 m in the Gulf of Lions (ST1, Table S1, Fig. 3). The nitracline was shallow in the Provençal Basin (50 – 60 m), dropping down in the Eastern Algerian and Tyrrhenian at 70 m; it was the even deeper in the Western Algerian and Ionian (80 – 90 m). Some anomalies 400 appeared on this progressive deepening of the nitracline from northwest to east and southwest, likely due to mesoscale activity (end of FAST and ST10), or a situation close to the continental shelf (ST3). Mean NDLb NO₃ concentrations ranged from detection limits using LWCC technique (9 nM) to 116 nM (Table S1, Fig. 4). In the ML, mean NO₃ concentration ranged from 9 to 135 nM. Note that mean NO₃ concentration was not systematically low 405 within the ML, particularly at FAST, ION and ST10. For the stations 5, TYR, 6, 7, ION25 May, FAST+1.05, FAST+2.1 (hereafter ‘group 1’), the nitrate concentrations were low (below 50 nM) in both ML and NDLb layers, with weak differences between the two layers. For the ST8 and the casts done before the rain event at FAST (hereafter ‘group 2’), the nutrient concentrations were moderate (50 - 80 nM) both in ML and NDLb with weak 410 difference between the two layers, indicating small gradients between ML and NDLb and thus, likely little instantaneous exchanges (at the time of the cast). For ST9, higher nitrate concentrations were measured in both ML and NDLb (> 80 nM) but the weak positive differences (< 20 nM) between the two layers also likely indicate weak or null exchanges between the two layers at the time of the cast (hereafter ‘group 3’). For ST10, ION27 and 415 ION29 May, and FAST+0.25, +0.5 and +3.8 (hereafter ‘group 4’), high and moderate nitrate concentrations were measured in the ML and NDLb, respectively, with a large positive difference (> 20 nM) between both layers.
Concerning DIP, nanomolar data indicated the presence of positive vertical gradients above the phosphacline, in all stations of the transect, so that DIP in the ML was always lower than 420 in the PDLb above except at ION and ST6 (where no gradient was detected) (Pulido-Villena et al. this issue, in prep.).



The vertical distribution of PP and BP are described in Marañón et al. (2020) for the short stations. Briefly, PP exhibited a deep maximum close to the DCM depth or slightly above whereas vertical distribution of BP generally showed 2 maxima, one within the mixed layer, 425 and a second one close to the DCM. Integrated PP (Table 1) ranged from 138 (TYR17 May) to 284 (SD1) $\text{mg C m}^{-2} \text{ d}^{-1}$ (mean \pm sd: $194 \pm 48 \text{ mg C m}^{-2} \text{ d}^{-1}$). Integrated BP (0-200 m) ranged from 44 (ION27may) to 113 (FAST+0.53) $\text{mg C m}^{-2} \text{ d}^{-1}$ (mean $70 \pm 20 \text{ mg C m}^{-2} \text{ d}^{-1}$).
430 The typical states in absence of rain event follow the west-east gradient of MS oligotrophy detected by ocean color (see Fig. 8 in Guieu et al., 2020), from 'chlorophyll-rich' waters encountered along the Algerian basin until 'chlorophyll-poor' waters in the Tyrrhenian Sea and 'ultra-poor' surface water in the Ionian Sea.
435 VmLAP at 5 m depth ranged from 0.24 to 0.56 nmol MCA-leu hydrolyzed $\text{l}^{-1} \text{ h}^{-1}$, and Km LAP ranged from 0.12 to 1.29 μM . The mean TAA within the ML ranged 0.17 to 0.28 μM . From these 3 series of parameters, we derived mean *in situ* LAP hydrolysis rate within the 440 ML, which ranged from 0.07 to 0.29 nmol $\text{N l}^{-1} \text{ h}^{-1}$ (results not shown but detailed in Van Wambeke et al., 2020).

3.2 N budgets and fluxes at short stations

Focusing on the surface mixed layer, biological rates, all expressed in N units, were 440 calculated as described in Material and Methods section and compared among the short stations ST1 to ST10 (Table 2). Phytoplankton N demand (phytoN demand) was the largest rate, followed by heterotrophic prokaryotic N demand (hprokN demand), *in situ* LAP hydrolysis rates and N_2 fixation. On average, phytoN demand was 2.9 fold higher than hprokN demand, ~~however~~ with a large variability (min x1.5, max x8.1). LAP hydrolysis rates 445 represented between 14 and 66 % of the hprokN demand, N_2 fixation rates represented from 1 to 4.5% of the phytoN demand.
450 Dry atmospheric deposition of inorganic N (DIN=NO₃+NH₄) was dominated by NO₃, which represented on average 79% of the total inorganic N (Table 2). The estimated inputs of DIN from dry deposition ranged from 17 to 40 $\mu\text{mol N m}^{-2} \text{ d}^{-1}$ with highest fluxes ($> 35 \mu\text{mol N m}^{-2} \text{ d}^{-1}$) at ST3 and ST9. Dry deposition of DIN was similar or higher than N_2 fixation rates in the ML (from 1.3 fold to 11 fold higher, mean 4.8 fold higher). On average, dry deposition of inorganic N represented 27% of the hprokN demand within the ML (range 10-82%), and 11% of the phytoN demand within the ML (range 1-30%).



455 **3.3 Biogeochemical evolution at the long station ION**

The ION site was occupied from the 25 to the 29 May, and the rain event occurred just 3 hours before the last CTD cast. However, rain events in the area of the site have been also observed on the day of May 26. CTD casts dedicated to biogeochemical studies were separated by 24 h (biological fluxes) or 48 h (DIP and NO₃). Thus the time sequence of nutrients at ION is given only by three profiles. The first profile (25 May) is 'flat', corresponding to fair weather conditions and shallow ML with low and homogeneous concentrations of NO₃ in the ML and the NDLb layers (Fig. 4). In the interval with the second profile, a depression arrived and the ML started to deepen 13 h before the second cast (27 May). This cast was marked by high nitrate in the ML, which is portioned at 10 m due to the history of the MLD (Fig. 3). The mixing should have set up homogeneous ML, but wind conditions rose at 20 kt just at the time of the cast (Fig. 3). The interval with the third cast (29 May, sampled 3 hours after the rain) is marked by slight relaxation of weather depression, and the deepening of ML down to 20 m. On 29 May, NO₃ decreased in both ML and NDLb but still, values were higher in ML. Given the remaining signature at 15 m and deepening of the ML, the two layers might have stayed isolated. However, the calculation of vertical advective fluxes between the layers showed a downward flux in the first interval 25-27 May (Fig. 4, Table S1) and an upward flux in the second interval (27-29 May). DIP dry atmospheric deposition decreased from 383 and 385 nmol P m⁻² d⁻¹ on the 26 and the 28 May down to 185 nmol P m⁻² d⁻¹ the 30 May. The percentage of DOP included in rain was also an important P source representing 60% of total dissolved P deposition. DIN (NO₃+NH₄) dry atmospheric fluxes could be sampled and daily flux calculated more regularly: it increased from 24 to 34 $\mu\text{mol N m}^{-2} \text{d}^{-1}$ from the 25 to the 28 May and decreased to 29 $\mu\text{mol N m}^{-2} \text{d}^{-1}$ on the 29 May after the rain. The rain sample was associated with a rain front covering more than 5 000 km² around the sampling zone, and passing during the night between 28 and 29 June. The rain event collected on board at ION lasted 52 min (Table 3). The DIN wet deposition flux was much higher than DIP flux, resulting in a molar N/P inorganic ratio of 208. As only one cast was sampled after the rain, we could not analyze the fate of this wet event in particular its possible effect on biological stocks and fluxes as a function of time.

485 Due to the lack of a high frequency sampling, it was also particularly difficult to assess direct time evolution effects of dry atmospheric deposition at ION site. Nevertheless, it was clear from the casts sampled on the 27 and 29 May that this site was characteristic of group 4 (i.e.



higher NO₃ in the ML than in the NDLb), indicating recent inputs from the atmosphere. The integrated BP increase within the ML indicates that hprok benefited more from the atmospheric inputs than PP which decreased at 5 m depth (Fig. S1).
490 At ION site, ectoenzymatic activities were only sampled on the 25 May. Vm of LAP at 5 m (0.22 nmol N l⁻¹ h⁻¹) was mostly one of the lowest values recorded during the cruise (min-max range of 0.21-0.56 nmol N l⁻¹ h⁻¹ for the whole cruise) and Vm of AP showed the highest value (5.6 nmol P l⁻¹ h⁻¹, for a min-max range of 0.3-5.6 nmol P l⁻¹ h⁻¹ for the whole cruise).
495 PP integrated over the euphotic zone increased slightly from 211 (25 May) to 282 mg C m⁻² d⁻¹ (28 May), but due to changes in the MLD during the occupation of the ION site (range 11-21 m) this trend was not visible when integrating over the ML. Integrated BP (0-200 m) ranged 43-63 mg C m⁻² d⁻¹ with the highest value on the 28 May. Integrated over the ML, BP slightly increased, from 7.5 to 10.3 mg C m⁻² d⁻¹ between the 25 and the 29 May. The profiles 500 of hprok and *Synechococcus* abundances showed no particular trend with time, with higher variations within the DCM (Fig. S1).

3.4 N budgets and fluxes at the long station FAST

During the occupation of the FAST site, NO₃ concentration in the ML showed a progressive enrichment with a maximum few hours after the rain event and a smooth decline until the initial conditions were restored 2.3 days after the rain (Fig. 3). Afterwards, the nutrient dynamics was not consistent with this evolution as shown by the high concentrations measured at FAST+3.8. The same analysis can be drawn with respect to exchanges across the ML (Fig. 4, Table S1): NO₃ flux remained low until the rain event, and then a large advective flux is estimated relative to the enrichment of ML and the quick deepening of the ML, this flux declined during the relaxation to initial conditions.
510

Concerning atmospheric wet deposition, the rain event collected on board at FAST lasted 28 min (Table 3). Like for the rain sampled at ION site, DIN flux was much higher than DIP flux, with molar N/P inorganic ratio of 1439, and the percentage of DOP represented 44% of 515 total dissolved P deposition. The chemical composition indicates that the rain sample collected at FAST site was characteristic of a wet dust deposition (Fu et al., this issue, in prep. b) corresponding to a dust deposition of 12 mg m⁻². This is among the least intense dust deposition fluxes recorded in this area from a long time-series of deposition (Vincent et al., 2016). During FAST site occupation, two periods of rains occurred related to rain fronts 520 (affecting a domain of ~5000 km²) moving eastward from Spain and North Africa regions:



between the evening of June 3 until 5 in the early morning (Desboeufs et al., this issue, in prep.). These two episodes were concomitant with a dust plume transported in altitude (between 1 and 4 km), covering the half of western Mediterranean basin during June 4, and allowed below-cloud deposition of dust (as confirmed by LIDAR records, Desboeufs et al., this issue, in prep.). The rain event collected at FAST site occurred on board after a first night of wet deposition over the whole area and toward the end of the transport of the dust plume. The particulate flux of this collected rain sample was thus likely in the lower range of the wet dust deposition fluxes that had affected the whole area between 3 and 5 June. Indeed, the *in situ* measurements of a dust tracer in the water column (particulate aluminum) show that the total export of particulate matter was rather of the order of $\sim 55 \text{ mg m}^{-2}$ during the period instead of 12 mg m^{-2} as seen in a single collected rain event, and even this value is probably underestimated due to the lack of sampling big dust particles sinking (Bressac et al., this issue, in prep.). After the rain, average daily dry DIN deposition decreased from $45 \text{ } \mu\text{mol N m}^{-2} \text{ d}^{-1}$ on the June 4 (4:00-17:00), to $27 \text{ } \mu\text{mol N m}^{-2} \text{ d}^{-1}$ on the following night (June 4 21:00 - June 5 4:40) and $9.8 \text{ } \mu\text{mol N m}^{-2} \text{ d}^{-1}$ on June 5 (9:20-15:00). The beginning of the sequence at FAST site (-2.3; -1.5; -0.25) was marked by moderate decreases of NO₃ concentration but with equal concentrations in the ML and NDLb. This stage reached a steady state after 2 days of evolution (means of 59 and 56 nM NO₃ at FAST-1.5 and FAST-0.25). Integrated stocks of NO₃ within the ML reflected slight changes in the ML depth (from 14 to 10 m during that time). The rainfall (rain 2, Table 3) was associated with a strong wind burst and an abrupt mixing. The two closest CTD casts framing the rain were sampled 6 h before and 6 h after (FAST-0.25 and FAST+0.24) and the comparison between both casts showed a clear enrichment of the ML: mean NO₃ increased from 56 to 93 nM and integrated stocks increased by $888 \text{ } \mu\text{mol N m}^{-2}$. In addition, there was a clear difference in the mean concentrations between ML and NDLb layers (93 ± 15 vs $51 \pm 7 \text{ nM}$, respectively, which is the highest difference between these 2 layers observed during the cruise), confirming that this ML enrichment could not be attributed to inputs from below. The relaxation of this wind burst was progressive, with a continuous deepening of the ML. The export of the nitrate from atmospheric input into the NDLb was maximum after the rain event (FAST+0.24). A much smaller value was recorded at FAST 2.1 and fluctuated not significantly differently than 0 in between.



The end of the sequence (FAST+3.8) was marked by the return of higher NO₃ (135 nM) content inside the ML. However this event can be isolated from the previous sequence and 555 more difficult to interpret as persistence timescales (about 2 days in the hypotheses) are over. If the NO₃ stocks inside ML were already increasing 6 h after the rain event, ~~however, it was~~ not the case for DIP which showed similar ML-integrated data 6 h before and 6 h after the rain (136 $\mu\text{mol m}^{-2}$) and then progressively increased up to 281 $\mu\text{mol P m}^{-2}$ at FAST+1 (1 day after the rain).

560 Immediately after the rain, integrated PP (euphotic zone) decreased from ~~FAST-0.9~~: 274 mg $\text{C m}^{-2} \text{ d}^{-1}$ to ~~FAST+0.07~~: 164 mg $\text{C m}^{-2} \text{ d}^{-1}$ and continued to decrease the following day (FAST+1.07: 140 mg $\text{C m}^{-2} \text{ d}^{-1}$). It is only after 3.8 days after the rain that integrated PP was of the same order of magnitude as before the rain. Such variations were mostly due to changes 565 in volumetric rates within the DCM depth (Fig. S2), as the activity did not change significantly within the ML (28-33 mg $\text{C m}^{-2} \text{ d}^{-1}$, Fig. S2, Fig. 5). Integrated BP 0-200 m showed an opposite trend compared to PP, ~~and tended to increase after the rain: 86 \pm 3 mg $\text{C m}^{-2} \text{ d}^{-1}$ (n = 4) before, and an increase from 80 (FAST+0.07) to 113 mg $\text{C m}^{-2} \text{ d}^{-1}$ (FAST+0.5) after.~~ The trend of increase was slight, but also visible when considering only ML (12-15 before; 15-19 $\text{m}^{-2} \text{ d}^{-1}$ after). The abundances of picophytoplankton groups were mostly 570 varying around the DCM depth with peaks occurring 1-2 days after the rain (grey profiles, Fig S3), in particular for prokaryotes (*Prochlorococcus*, *Synechococcus*). Heterotrophic prokaryotes and nanoflagellate abundances slightly ~~also~~ increased within the DCM depth after the rain.

575 **3.5 Enrichment experiments at long stations**

At TYR site, BP was significantly stimulated only after addition of 2 major elements, with a greater response with PN and NPG combinations (Fig. 6). At ION site, BP was primarily limited by P availability, as only ~~combinations with P~~ single or in combination with other elements, stimulated BP whereas all other combinations of enrichment did not stimulate BP 580 significantly compared to the control. At FAST site, BP was primarily limited by N availability, as all combinations with N, single or in combination with other elements, stimulated BP. However at this site it is likely that BP was also co-limited by 2 elements, as G addition alone also stimulated BP. Note that the PN combination has induced a higher stimulation of BP than other double combinations (NG or PG).

585



4. Discussion

In this study, *in-situ* characterization of the biogeochemical response to atmospheric deposition was studied for the surface mixed layer (ML) at the interface with the atmosphere.

590 The specific context of the oceanographic survey constrained the data analysis: biogeochemical responses to a rain event have been scaled in time over a few days (3 - 5), and in space spanning tens of km (40 - 50). Their evolution was restricted to the vertical dimension, integrating lateral exchanges by horizontal diffusion or local advection that occurred at the prescribed space and time scales. In the vertical dimension, exchanges of

595 nutrients across the ML were controlled by advection due to rapidly changing conditions (MLD fluctuations and nutrient inputs from the atmosphere) rather than diffusion between stationary pools.

In this context, we will i) discuss the classification of stations according to gradients of NO₃ concentrations between the ML and the NDLb, ii) discuss the nitrogen budget within the ML

600 at the short stations considered as 'snapshot', and iii) analyze finely, using a time series of CTD casts, biogeochemical changes within the ML and the NDLb following the atmospheric wet deposition event at FAST site along with the possible modes of transfer of nutrients between these 2 layers.

605 **4.1 NO₃ dynamics in the ML**

Four different groups of stations corresponding to different stages of ML enrichment and relaxation, due to the nutrient inputs from single rain events, have been characterized using the qualitative assessment described in section 2.4, i.e. the differences in NO₃ concentration between ML and NDLb. As shown in Fig. 4, this succession of stages is in agreement with the

610 NO₃ fluxes from above and below the ML. Moreover, they provide a temporal scaling of the oceanic response to atmospheric deposition, with a quasi-instantaneous change at the time of the rain event and a 2-days relaxation period to recover pre-event conditions. In terms of spatial scale, although a single rain event was collected on board at ION and FAST sites, the rain radar data indicated the presence of a rain front, including numerous rain events with

615 abundant rainfalls that occurred in a larger area surrounding the ship location. This happened at ION during the second and third days of sampling (26-27 May), although two short rain events occurred onboard the ship; only the significant rainfall was collected at the end of this



site (29 May). The chemical composition of the rain indicated that the rain sample collected at ION was under anthropogenic background influence (Fu et al., this issue, in prep. b).

620 At FAST site a rain occurred around the ship on 4 June while rainfall was sampled onboard only during the night between June 4 and 5. The dust deposition flux estimated from the rain sampled on board was 12 mg m^{-2} which is among the least intense dust deposition fluxes recorded in this area from a long time-series of deposition (Vincent et al., 2016). We believe that the biogeochemical response measured was not only due to a localized event collected on board but rather was the results of a suite of atmospheric events that had impacted the ML nutrient contents under the effect of horizontal mixing with a spatial range of the order of the oceanic mesoscale. This is in agreement with the lagrangian analysis of the surface flow at FAST (Figs 5 and 12 in Guieu et al. 2020). The evolution of the ML nutrient is indeed certainly not only linked to the single isolated wet deposition collected onboard but integrates 630 the total wet atmospheric inputs, spatially patchy over a larger area ($\sim 40\text{-}50 \text{ km radius}$ around the R/V). However, the chemical characteristics of collected rain probably provide a good picture of the rain waters composition in the rain fronts.

4.2 A snapshot of biological fluxes in ML and their link to dry atmospheric deposition

635 Enrichment experiments undertaken at the 3 long sampling sites indicated that either single, or co-limitation by N, P occurred among hprok in the ML (Fig. 6). The dependence of hprok on nutrients rather than on labile organic carbon sources suggests that they largely compete with phytoplankton for inorganic nutrients. This is consistent with other studies in the MS (Van Wambeke et al., 2002, Céa et al., 2017; Sala et al., 2002). Under such conditions of 640 limitation, ~~it is thus probable~~, due to the advantage of their small- sized cells and kinetic systems adapted to low concentration ranges of nutrients (for example for DIP see Talarmin et al., 2015), ~~that~~ hprok will ~~react~~ rapidly to new phosphorus and nitrogen inputs, ~~like those~~ coming from the atmosphere. During an artificial *in situ* DIP enrichment in Eastern Mediterranean, P rapidly circulated through hprok and heterotrophic ciliates, while the 645 phytoplankton was not directly linked to this 'bypass' process (Thingstad et al., 2005). Bioassays conducted in the tropical Atlantic Ocean have also shown that hprok respond more strongly than phytoplankton to Saharan aerosols (Marañón et al. 2010), a pattern that has been confirmed in a meta-analysis of *in vitro* dust addition experiments (Guieu et al. 2014a).



650 We considered hprokN demand together with phytoN demand and compared it to autochthonous (DON breakdown by ectoenzymatic activity) and allochthonous sources (atmospheric deposition). To our knowledge this is the first time that these fluxes are compared based on their simultaneous measurements on board. A high variability was observed among the 10 short stations (Table 2). The regeneration of nitrogen through 655 aminopeptidase activity was clearly the first provider of N to hprok: 14 to 66% of the hprokN demand could be satisfied by *in situ* LAP activity. Such percentages may be largely biased by the conversion factors from C to N and propagation of errors for the LAP hydrolysis rates and BP rates. However, the C/N ratio of hprok is relatively narrow under large variations of P or N limitation (6.2 to 8.4; Nagata 1986).

660 Other regeneration sources exist like direct excretion of NH4 or low molecular weight DON source with no necessity of hydrolysis prior to uptake (Jumars et al., 1989). For instance, Feliú et al. (2020) calculated that NH4 and DIP excretion by zooplankton would satisfy 25- 665 43% and 22-37% of the whole euphotic zone phytoN demand and phytoP demand, respectively. Such percentages suggest that direct excretion by zooplankton in addition to ectoenzymatic activity, also substantially provides N for biological activity.

N₂ fixation can also fuel hprok directly as some are heterotrophic diazotrophs (Delmont et al. 2018, and references therein), or indirectly, as part of the fixed N₂ rapidly cycles through hprok (Caffin et al., 2018). Furthermore, a better coupling of N₂fix rates with BP rather than with PP has been observed in the eastern MS (Rahav et al., 2013a). For this reason, we also 670 examined a hypothetical contribution of N₂fix rates to hprokN demand: it was low, ranging from 1 to 4.5 %. It is consistent with the low N₂fix rates observed in the MS (i.e. Rahav et al., 2013b; Ibello et al., 2010; Ridame et al., 2011; Bonnet et al., 2011), in comparison to oceans 675 primarily limited by N but not P, such as the south eastern Pacific where N₂fix rates are high (Bonnet et al., 2017) and can represent 3 to 81 % of the hprokN demand (Van Wambeke et al., 2018).

Considering LAP as the most relevant regeneration N source, it is clear that even the sum of LAP activity and N₂ fixation were not sufficient to meet hprokN demand (cumulated, those fluxes contributed 19 to 73% of HbactN demand). With hprok primarily limited by the availability of N, P or colimited NP, we thus examined possible N sources provided by the 680 atmosphere (P sources at the short stations are discussed in Pulido-Villena et al, this issue, in prep.). Dry atmospheric DIN deposition fluxes ($29 \pm 7 \mu\text{mol N m}^{-2} \text{ d}^{-1}$ at the short stations) were among the lowest recorded for the Mediterranean but were obtained offshore compared



to other measurements carried out at coastal sites where local/regional contamination contribute significantly to the flux (Desboeufs, in press). On a yearly survey, based on 10 685 aerosols collectors all around coastal sites of the Mediterranean Sea, dry DIN deposition was very patchy in space and time with an average of $38 \mu\text{mol N m}^{-2} \text{d}^{-1}$ (Markaki et al., 2010). Nevertheless, atmospheric deposition fluxes also include organic matter (Djaoudi et al., 2017, Kanakidou et al., 2018), which is bioavailable for marine hprok (Djaoudi et al., 2020). Soluble DON from aerosols was unfortunately not determined here. DON solubilized from 690 aerosols contributes 19 to 42% of the total N dry deposition in MS (Desboeufs, in press; Galletti et al., 2020). Considering a mean of 32%, DON dry deposition ranged from 8 to $19 \mu\text{mol N m}^{-2} \text{d}^{-1}$ at the short sampling stations. The total N flux provided by the dry atmospheric deposition (inorg+org) would represent from 14 to 121% of hprokN demand. Such concomitant measurement confirmed the great spatial variability of the different 695 contributions. Such percentages can be biased by the assumptions on the deposition velocity used. We considered averages deposition velocity set at 1 cm sec^{-1} for NO₃ and 0.21 cm sec^{-1} for NH₄. As NO₃ was dominating inorganic dry deposition, it is clear that the choice of 1 cm sec^{-1} for NO₃ influenced largely its contribution. This choice is conditioned by the predominance of NO₃ in the large mode of Mediterranean aerosols as dust or sea salt particles 700 (e.g. Bardouki et al., 2003). However, the deposition velocity of NO₃ between fine and large particles could range from 0.6 to 2 cm sec^{-1} in the Mediterranean aerosols (e.g. Sandroni et al., 2007). Even considering the lower value of 0.6 cm sec^{-1} from the literature, the contribution of atmospheric dry deposition to hprokN demand within the ML would still be significant, and up to 72%.

705

We examined if the four groups of stations described in results section 3.1 and based on NO₃ distribution were also characterized by particular biological fluxes. Although a large variability of biological activities were observed in the ML among these 4 groups, some trends were depicted. LAP activity in ML was higher at the stations of group 1 (with lowest 710 NO₃ concentration in ML and NDLb), in comparison to the group 4 (which exhibited the larger difference of concentrations between ML and NDLb) (121 ± 54 compared to $46 \pm 23 \mu\text{mol N L}^{-1} \text{d}^{-1}$, respectively). The stations from group 1 also presented the lowest DIN dry deposition flux ($26 \pm 6 \mu\text{mol N m}^{-2} \text{d}^{-1}$). Finally, it was always in a station from group 4 that the higher phytoN demand, HbactN demand and N2fix rates were detected. Part of the 715 variability obtained among the different groups was also related to the instantaneous character



of comparison. Indeed, it is clear that a succession of biogeochemical changes occurs at different time scales during an atmospheric deposition event. Such comparison as a function of time was possible at station FAST and will be discussed below.

720 **4.3 Biogeochemical response after a wet event – N and P budgets at FAST site**

Rain events are more erratic than dry atmospheric deposition but provide on average much higher nutrient fluxes on an annual basis, e.g. 84% of DIN fluxes in Corsica Island (Desboeufs et al., 2018). At the scale of Mediterranean basin, the annual wet deposition of DIN was found to be 2-8 times higher than that of dry deposition (Markaki et al., 2010). Wet 725 deposition contributes also significantly to DON atmospheric fluxes in the MS: total (wet + dry) DON atmospheric fluxes ranges between 7 and 367 $\mu\text{mol DON m}^{-2} \text{ day}^{-1}$ in the NW MS (Frioul Island; Djaoudi et al., 2018) and between 1.5 and 250 $\mu\text{mol DON m}^{-2} \text{ day}^{-1}$ in the Eastern MS (Lampedusa Island; Galetti et al., 2020), with DON contribution to the total nitrogen flux of $41 \pm 14\%$ and 25%, respectively (Djaoudi et al., 2018; Galletti et al., 2020).
730 In both studies, bulk atmospheric fluxes of DON were positively correlated with precipitation rates, indicating the preponderance of wet deposition over dry deposition.

The coupled atmospheric and biogeochemical water column sampling time series at FAST site was based on casts performed before and after a single rain collected on board ~~on the 735 5/6/2017 at 3:04, and lasting for 28 min~~. The maximum net accumulation of NO₃ and DIP within the ML after the rainy period reached i) $1520-665=855 \mu\text{mol N m}^{-2}$ for NO₃ (~~data from FAST +0.24 relative to FAST 0.25 and~~ ii) $283-137=144 \mu\text{mol P m}^{-2}$ for DIP, (~~data from FAST +1.05 relative to FAST 0.25~~). In other terms, based on a mean MLD of 16 m, the rain collected on board would have delivered 0.008 nM DIP and 7 nM NO₃ over the whole mixed 740 layer. The net observed accumulations in the ML (5 nM DIP and 38 nM NO₃) are thus much higher than the calculated variation in stocks deduced from the N and P concentrations of this collected rain (Table 4). This is still true when including all P or N chemical forms (dissolved and particulate inorganic + organic). For instance for P, the total atmospheric deposition would increase by ~ 0.07 nM the P concentration in the ML. One reason for this discrepancy 745 might be, as developed in section 3.4, that the collected rain sampled on board represented only a fraction of the whole rain episode that affected a large area around the ship. Based on aluminum inventory in the water column (Bressac et al., this issue, in prep.), the total dust deposition having affected the FAST site was 4.6 times higher (55 mg m^{-2}) than the dust flux



measured from our single rain event (12 mg m^{-2}). It is likely that the deduced new N and P increases within the ML due to the collected rain are well underestimated. If we consider the above cited factor of 4.6, the atmospheric flux could have provided an addition of about 33 nM for NO_3 and 0.037 nM for DIP (0.35 nM total P) in the ML, more in agreement with the marine volumetric variation, at least for NO_3 , and suggesting even that atmospheric nitrate input could alone explain the increase of NO_3 in the ML.

A delay of about 19 h was observed in the maximum net accumulation within the ML between DIP (FAST+1.05) and NO_3 (FAST+0.24). The DIN/DIP ratio in the rain (1438) was much higher than Redfield ratio. As the biological turnover of DIP in the Mediterranean Sea is rapid (from min to few h, Talarmin et al., 2015), this indicates that DIP provided by rain might have behaved differently than DIN. Two different mechanisms can be proposed to explain the observed delay: (i) processes linked to bypasses and luxury DIP uptake (storage of surplus P in hprok before a rapid development of grazers (Flaten et al., 2005; Herut et al., 2005, Thingstad et al., 2005) that are later on, responsible for a DIP regeneration process so that DIP net accumulation is delayed and/or (ii) abiotic processes such as rapid desorption from large sinking particles followed by adsorption of DIP onto submicronic iron oxides still in suspension as evidenced experimentally in Louis et al. (2015). The first proposed mechanism may be supported by the observed increase of BP, along with a stable PP which suggests an immediate benefit of the new nutrients from rain by hprok rather than phytoplankton. The so-called luxury DIP uptake is efficient by competing organisms like hprok (small cells with high surface/volume ratio and DIP kinetic uptake adapted to low concentrations). It is of course difficult to quantify such variation *in situ* in comparison to mesocosms/minicosms dust addition experiments, in which clearly heterotrophy is favored first (Marañón et al., 2010; Guieu et al., 2014b; Gazeau et al., 2020). Few attempts in the field have been already described, confirming these trends (Herut et al., 2005, Pulido-Villena et al., 2008) but, as described in the introduction, those studies lacked high frequency sampling. The second proposed mechanism, the abiotic desorption/adsorption, is compatible with the observed 19 h delay (Louis et al. 2015). Note however that most of the estimates of such abiotic processes are from dust addition experiments with contrasting results, some showing this abiotic process of absorption/desorption while the particles are sinking (Louis et al., 2015), and other not (Carbo et al., 2005) or showing it as negligible in batch experiments (Ridame et al., 2003). Using natural or artificial dust for enrichment experiments in abiotic



conditions is not simple to realize, or to interpret. It is possible that DIP adsorbed onto large particles rapidly sinks out of the ML, and desorb partly during their transit in the PDLb, where they could stay longer thanks to the pycnoclines barriers.

785 We tentatively made a P budget: between FAST+1.05 and FAST+2.11 a net decrease of DIP ($-87 \mu\text{mol P m}^{-2}$) was observed in the ML. During that time, advective flux of DIP toward the PDLb was not detectable as DIP concentration within the ML was always lower than within the PDLb (Pulido-Villena et al., this issue, in prep.). This indicated that this DIP was assimilated and/or transformed to DOP via biological processes, and/or adsorbed onto
790 particles and then exported to PDLb by sedimentation. We integrated PP and BP over that period (34.5 and 19.7 mg C m^{-2} , respectively) and, assuming that all the $87 \mu\text{mol DIP m}^{-2}$ disappearing would be consumed by these organisms, we could estimate a C/P ratio reached in their biomass of $((34.5+19.7)/12*1000)/87=52$ which indeed suggests that DIP was not limiting these organisms anymore. Indeed a decrease of C/P quotas may highlight a switch
795 from P to C limitation for heterotrophic bacteria (Godwin and Cotner, 2015) and from P to N limitation or increased growth rates for phytoplankton (Moreno and Martiny, 2018). Furthermore, as DIP is also recycled via alkaline phosphatase within the ML, we consider also another source of DIP via alkaline phosphatase activity, from which *in situ* activity (see Van Wambeke et al., 2020 for *in situ* estimates) could release $139 \mu\text{mol DIP m}^{-2}$ during that period. Assuming also that DIP resulting from AP hydrolysis was fully assimilated for P biological needs, then C/P ratio would be $((34.5+19.7)/12*1000)/(87+139)=19$. This low ratio seems unrealistic for phytoplankton (Moreno and Martigny, 2018) as well as hprok, even growing in surplus C conditions (Makino et al., 2003; Lovdal et al., 2008; Godwin and
800 Cotner, 2015). DIP is abiotically adsorbed on mineral dust particles (Louis et al., 2015), most of them sinking, and thus constitute a source of export out of the ML. It is also possible, however, that such sorbing process on dust particles allow export of other P-containing organic molecules, as for instance DOP or viruses produced after luxury DIP assimilation. Free viruses, richer in P than N relative to Hprok, could adsorb, like DOM, on dust particles and constitute a P export source. Indeed, free viruses sorb on black carbon particles, possibly
805 reducing viral infection (Mari et al., 2019; Malits et al., 2015). However, particle quality is a determining factor for DOM or microbial attachment, and what has been shown for black carbon particles is not necessarily true for dust particles. For instance the addition of a Saharan dust to marine coastal waters led to a negligible sorption of viruses to particles and increased abundances of free viruses (Pulido-Villena et al., 2014), possibly linked to an



815 enhancement of lytic cycles in the ML after relieving limitation (Pradeep Ram and Sime-Ngando, 2010).
We are aware of all the assumptions made here ((i) conversion factors, (ii) *in situ* estimates of alkaline phosphatase, (iii) some missing DIP source in the budget, such as the excretion of zooplankton estimated to amount 22–37% of the phytoP demand at FAST (Feliú et al., 2020),
820 iv) lack of knowledge on the different mechanisms linking P to dust particles, and (iv) the hypothesis considering the station as a 1D system. Nevertheless, all these results together suggest that both luxury consumption by Hprok and export via scavenging on mineral particles, likely occurred simultaneously to explain the observed variations of DIP in the ML.

825 For NO₃, and in opposition to the observations for DIP, we observed physical exchanges by advection between ML and NDLb. Indeed, NO₃ was higher within the ML than within the NDLb at FAST+0.24 and FAST+0.53 and then NO₃ was lower within the ML than within NDLb at FAST+1.05 and FAST+2.11, suggesting a rapid transfer of NO₃ in the NDLb. As for DIP, we made ~~an~~ N budget within the ML during the period of net NO₃ decrease (1520; 830 1113; 852 and 177 $\mu\text{mol N m}^{-2}$ at FAST+0.24, FAST+0.5, FAST+1.05 and FAST+2.11, respectively). This indicates a net loss of 1343 $\mu\text{mol N m}^{-2}$ in 1.8 days within the ML. Over these 1.8 days, the time-integrated phytoN and hprokN demands were 682 $\mu\text{mol N m}^{-2}$ and 378 $\mu\text{mol N m}^{-2}$, respectively, so that total biological demand in ML was 1060 $\mu\text{mol N m}^{-2}$. During this period, possible N sources used were stocks of NO₃ disappearing (net diminution 835 assumed to be consumption = 1343 $\mu\text{mol N m}^{-2}$), as well as N₂ fixation and *in situ* aminopeptidase activity which fluxes integrated over that period of time were 13 and 87 $\mu\text{mol N m}^{-2}$, respectively, i.e. a total possible source of N amounted 1443 $\mu\text{mol N m}^{-2}$. Keeping in mind that the same potential caveats (see above) apply also for the calculation of N budget, the biological N demand appeared thus lower than the sources (difference ~380 $\mu\text{mol N m}^{-2}$).
840 On the other hand at FAST, vertical advective fluxes of NO₃ were up to 337 $\mu\text{mol N m}^{-2} \text{ d}^{-1}$ (Fig. 4), i.e. ~600 $\mu\text{mol N m}^{-2}$ lost from the ML over 1.8 days. From these two different approaches, exported NO₃ should range between 380 and 600 $\mu\text{mol N m}^{-2}$ during that period. We could conclude that about one third of the NO₃ accumulated in the ML after the rain was exported by vertical advection to the NDLb. ~~This input of new nutrients could benefit~~
845 ~~organisms present at the DCM~~. Indeed, PP and abundances of all 4 phytoplankton groups (*Synechococcus*, *Prochlorococcus*, nano and picoeukaryotes) increased at the DCM, 1 or 2 days after the rain event and PP recovered its initial value before rain (Fig. S3). The increases



in abundances were higher for prokaryotic phytoplankton abundances, as such organisms would likely benefit from their small size and their ability to use DON/DOP organic molecules (Yelton et al., 2016).

850 5. Conclusions

This study reports for the first time simultaneous sampling of atmospheric and ocean biogeochemical parameters to characterize in-situ, in the context of an oceanographic cruise, 855 the biogeochemical responses to dust deposition within the ML. High-frequency sampling, in particular at the FAST site, confirmed the transient status of exchanges between the ML and the NDLb layers. Furthermore, the dust wet deposition event, as usual, was intermittent and patchy in space and time and we caught only one part of the deposition. We hypothesized a fully non-stationary and purely vertical evolution of the oceanic response, lasting for a few 860 days (48 h occupation of the FAST site) and spanning over 40 - 50 km. Under these assumptions, we assume our sampling representative of a wider-ranging water mass than the one crossed by the vessel, integrating every local patch of rain event (rather than only the one received onboard) thanks to horizontal oceanic stirring. Finally, the comparison with the mesocosms results (where the fertilization is more important due to high dust concentrations) 865 is hard to extrapolate with the ones presented here.

Nevertheless, our results showed the important role played by the ML in the biogeochemical and physical processes responsible for transfers of matter and nutrients between the atmosphere and the nutrient depleted layer below. Thanks to the uses of LWCC technique and access to nanomolar variations of NO₃ and DIP, it was possible to demonstrate the role of the 870 ML and exchanges of NO₃ from the ML to the NDLb by vertical advection when variations of ML depth occurred simultaneously to transitory accumulation of NO₃ after deposition event. As pictured on Fig. 7, this study confirms previous evidence that hprok in the ML and the presence of dust particles and mechanism of sinking adsorption/desorption play together a role in the transfer of P atmospheric deposition from the ML to the nutrient depleted layer. 875 Our results also show the time sequence occurring after a wet dust deposition event: accumulation of NO₃ in the ML, advection to NDLb, luxury consumption of DIP by hprok and delayed peaks of DIP, decrease of primary production and its recovery after 2 days mainly visible in the nutrient depleted layer. The effect of dust deposition is thus a complex and timely-controlled trophic cascade within the microbial food web. It showed the important



880 role of intermittent, but strong abiotic effects such as downwelled advective fluxes from the
ML to the nutrient depleted layers. It will be important to consider these aspects in budgets
and non stoichiometric models, especially when climate and anthropogenic changes are
predicted to increase aerosol deposition in the Mediterranean Sea.

885 **Acknowledgements** :This study is a contribution of the PEACETIME project
(<http://peacetimoproject.org>), a joint initiative of the MERMEX and ChArMEx components
supported by CNRS-INSU, IFREMER, CEA, and Météo-France as part of the programme
MISTRALS coordinated by INSU (doi: 10.17600/17000300). The research of EM was
funded by the Spanish Ministry of Science, Innovation and Universities through grant
890 PGC2018-094553B-I00 (POLARIS). The authors thank also many scientists & engineers for
their assistance with sampling/analyses: Marc Garel, Sophie Guasco and Christian Tamburini
for AP and LAP activity, Ruth Flerus for TAA, Joris Guittaneau and Sandra Nunige for
nutrients, Thierry Blasco for POC, Julia Uitz and Céline Dimier for TChl a (analysed at the
SAPIG HPLC analytical service at the IMEV, Villefranche), Philippe Catala for flow
895 cytometry analyses, Sylvain Triquet and Franck Fu for atmospheric particulate nitrogen and
phosphorus.



References

Aminot, A. and Kéroutil, R. : Dosage automatique des nutriments dans les eaux marines, in:
900 Méthodes d'analyses en milieu marin, edited by: IFREMER, 188 pp, 2007.

Bardouki, H., Liakakou, H., Economou, C., Sciare, J., Smolik, J., Zdimal, V., Eleftheriadis,
K., Lazaridis, M., Dye, C., and Mihalopoulos, N.: Chemical composition of size
resolved atmospheric aerosols in the eastern Mediterranean during summer and winter,
Atmos. Environ., 37, 195–208, 2003.

905 Bonnet, S., Grosso, O., and Moutin, T.: Planktonic dinitrogen fixation along a longitudinal
gradient across the Mediterranean Sea during the stratified period (BOUM cruise).
Biogeosciences, 8, 2257-2267, 2011.

Bonnet, S., Caffin, M., Berthelot, H., and Moutin, T.: Hot spot of N₂ fixation in the western
tropical South Pacific pleads for a spatial decoupling between N₂ fixation and
910 denitrification., PNAS letter, doi: 10.1073/pnas.1619514114, 2017.

Brainerd, K. E., and Gregg, M. C.: Surface mixed and mixing layer depths. Deep-Sea
Research Part I, 42(9), 1521–1543. doi: 10.1016/0967-0637(95)00068-H, 1995.

Bressac, M., Wagener, T., Tovar-Sanchez, A., Ridame, C., Albani, S., Fu F., Desboeufs, K.
and Guieu C.: Residence time of iron and aluminium in the surface Mediterranean Sea
915 (Peacetime cruise), this special issue, in preparation.

Caffin, M., Berthelot, H., Cornet-Barthaux, V., Barani, A., and Bonnet, S.: Transfer of
diazotroph-derived nitrogen to the planktonic food web across gradients of N₂ fixation
activity and diversity in the western tropical South Pacific Ocean, Biogeosciences, 15,
3795–3810, doi: 10.5194/bg-15-3795-2018, 2018.

920 Carbo, P., Krom, M. D., Homoky, W. B., Benning, L. G., and Herut, B.: Impact of
atmospheric deposition on N and P geochemistry in the southeastern Levantine basin,
Deep Sea Res. II, 52, 3041–3053. doi: 10.1016/j.dsr2.2005.08.014, 2005.

Céa, B., Lefèvre, D., Chirurgien, L., Raimbault, P., Garcia, N., Charrière, B., Grégori, G.,
Ghiglione, J.-F., Barani, A., Lafont, M., and Van Wambeke, F.: An annual survey of
925 bacterial production, respiration and ectoenzyme activity in coastal NW Mediterranean



waters: temperature and resource controls, *Environ Sci Pollut Res*, doi: 10.1007/s11356-014-3500-9, 2014.

Christaki, U., Courties, C., Massana, R., Catala, P., Lebaron, P., Gasol, J. M., Zubkov, M.: Optimized routine flow cytometric enumeration of heterotrophic flagellates using SYBR Green I, *Limnol. Oceanogr. Methods*, 9, doi: 10.4319/lom.2011.9.329, 2011.

930 de Boyer Montegut, C., Madec, G., Fisher, A. S., Lazar, A., and Iudicone, D.: Mixed layer depth over the global ocean: An examination of profile data and a profile-based climatology, *Journal of Geophysical Research. Oceans*, 109, C12003, doi: 10.1029/2004JC002378, 2004.

935 Delmont, T.O., Quince, C., Shaiber, A., Esen, Ö.C., Lee, S.T.M., Rappé, M.R., McLellan, S.L., Lücker, S. and Murat Eren, A.: Nitrogen-fixing populations of Planctomycetes and Proteobacteria are abundant in surface ocean metagenomes. *Nature Microbiology*, doi: 10.1038/s41564-018-0176-9, 2018.

940 Desboeufs, K.: Nutrients atmospheric deposition and variability, in *Atmospheric Chemistry and its Impacts in the Mediterranean Region* (ChArMex book), Springer, in press.

Desboeufs, K., Bon Nguyen, E., Chevaillier, S., Triquet, S., and Dulac, F.: Fluxes and sources of nutrient and trace metal atmospheric deposition in the northwestern Mediterranean, *Atmospheric Chemistry and Physics*, 18, 14477–14492, doi: 10.5194/acp-18-14477-2018, 2018.

945 Desboeufs, K., Doussin, J.-F., Giorio, C., Triquet, S., Fu, Y., Dulac, F., Garcia-Nieto, D., Chazette, P., Féron, A., Formenti, P., Gaimoz, C., Maisonneuve, F., Riffault, V., Saiz-Lopez, A., Siour, G., Zapf, P., and Guieu, C.: ProcEss studies at the Air-sEa Interface after dust deposition in the MEditerranean sea (PEAcEtIME) cruise: Atmospheric overview, this special issue, in preparation.

950 Dittmar, T.H., Cherrier, J. and Ludwichowski, K.-U: The analysis of amino acids in seawater. In: *Practical Guidelines for the Analysis of Seawater*, edited by: Wurl, O., Boca Raton, FL: CRC-Press, 67–78, 2009.

D'Ortenzio, F., Iudicone, D., de Boyer Montegut, C., Testor, P., Antoine, D., Marullo, S., Santoleri, R., and Madec, G.: Seasonal variability of the mixed layer depth in the



955 Mediterranean Sea as derived from in situ profiles., *Geophysical Research Letters*, 32, L12605, doi:10.1029/2005GL022463, 2005.

Djaoudi, K., Van Wambeke, F., Barani, A., Hélias-Nunige, S., Sempéré, R., and Pulido-Villena, E.: Atmospheric fluxes of soluble organic C, N, and P to the Mediterranean Sea: potential biogeochemical implications in the surface layer, *Progress in Oceanography*, 163: 59-69, MERMEX special issue, doi: 10.1016/j.pocean.2017.07.008, 2017.

960 Djaoudi, K., Van Wambeke, F., Coppola, L., D'ortenzio, F., Helias-Nunige, S., Raimbault, P., Taillandier, V., Testor, P., Wagener, T., and Pulido-Villena, E.: Sensitive determination of the dissolved phosphate pool for an improved resolution of its vertical variability in the surface layer: New views in the P-depleted Mediterranean Sea *Frontiers in Marine Science*, vol 5, article 234, doi: 10.3389/fmars.2018.00234, 2018.

965 Djaoudi, K., Van Wambeke, F., Barani, A., Bhairy, N., Chevaillier, S., Desboeufs, K., Nunige, S., Labiad, M., Henry des Tureaux, T., Lefévre, D., Nouara, A., Panagiotopoulos, C., Tedetti, M., and Pulido-Villena E.: Experimental evidence of the potential bioavailability for marine heterotrophic bacteria of aerosols organic matter, *Biogeosciences Discuss.*, bg-2020-187, 2020.

970 Du, C., Liu, Z., Kao, S.-J., and Dai, M.: Diapycnal fluxes of nutrients in an oligotrophic oceanic regime: The South China Sea. *Geophysical Research Letters*, 44, 11, 510–11, 518, doi: 10.1002/2017GL074921, 2017.

975 Feliú, G., Pagano, M., Hidalgo, P., and Carlotti, F.: Structure and functioning of epipelagic mesozooplankton and response to dust events during the spring PEACETIME cruise in the Mediterranean Sea, *Biogeosciences Discuss.*, <https://doi.org/10.5194/bg-2020-126>, 2020.

980 Flaten, G. A., Skjoldal, E. F., Krom, M. D., Law, C. S., Mantoura, F. C., Pitta, P., Psarra, S., Tanaka, T., Tselepidis, A., Woodward, E. M., Zohary, T., and Thingstad, T. F.: Studies of the microbial P-cycle during a Lagrangian phosphate-addition experiment in the Eastern Mediterranean, *Deep-Sea Res II*, 52, 2928–2943, 2005.

Fu F., Desboeufs K., Triquet S., Doussin J-F, Giorio C., Dulac F. and Guieu C.: Solubility and sources of trace metals and nutrients associated with aerosols collected during



985 cruise PEACETIME in the Mediterranean Sea, *Atmos. Phys. Chem.*, this special issue,
in preparation a.

990 Fu, F., Triquet, S., Tovar-Sánchez, A., Bressac, M., Doussin, J-F., Giorio C., Dulac, F., Guieu, C. and Desboeufs K. : Wet deposition of nutrients and trace metals in the Western and Central Mediterranean Sea: Background rain vs Rain dust, , *Atmos. Phys. Chem.*, this special issue, in preparation b.

Galletti, Y., Becagli, S., di Sarra, A., Gonnelli, M., Pulido-Villena, E., Sferlazzo, D. M., Traversi, R., Vestri, S., and Santinelli, C.: Atmospheric deposition of organic matter at a remote site in the Central Mediterranean Sea: implications for marine ecosystem, *Biogeosciences*, 17, 3669–3684, <https://doi.org/10.5194/bg-17-3669-2020>, 2020.

995 Gardner, W. D., Chung, S. P., Richardson, M. J., and Walsh, I. D.: The oceanic mixed-layer pump., *Deep-Sea Research II* 42, 757-775, 1995.

Gasol, J.M., and del Giorgio, P.A.: Using flow cytometry for counting natural planktonic bacteria and understanding the structure of planktonic bacterial communities, *Scientia Marina*, 64, 197-224, 2000.

1000 Gazeau F., Marañon E., Van Wambeke F., Alliouane S., Stolpe C., Blasco T., Ridame C., Pérez-Lorenzo M., Barbara Marie, Engel A., Zäncker B., & Guieu C. Impact of dust enrichment on carbon budget and metabolism of Mediterranean plankton communities under present and future conditions of pH and temperature, this special issue, in preparation.

1005 Godwin, C. M., and Cotner, J. B.: Aquatic heterotrophic bacteria have highly flexible phosphorus content and biomass stoichiometry, *the ISME Journal*, 9, 2324-2327, doi:10.1038/ismej.2015.34, 2015.

1010 Guieu , C., and Ridame, C.: Impact of atmospheric deposition on marine chemistry and biogeochemistry. In *Atmospheric Chemistry and its Impacts in the Mediterranean Region* (ChArMex book), Springer, in press.

Guieu, C., Dulac, F., Desboeufs, K., Wagener, T., Pulido-Villena, E., Grisoni, J.-M., Louis, J., Ridame, C., Blain, S., Brunet, C., Bon Nguyen, E., Tran, S., Labiad, M., and Dominici, J.-M.: Large clean mesocosms and simulated dust deposition: a new methodology to



investigate responses of marine oligotrophic ecosystems to atmospheric inputs,
1015 Biogeosciences, 7, 2765-2784, doi: 10.5194/BG-7-2765-2010, 2010.

Guieu, C., Aumont, O., Paytan, A., Bopp, L., Law, C. S., Mahowald, N., Achterberg, E. P.,
Marañón, E., Salihoglu, B., Crise, A., Wagener, T., Herut, B., Desboeufs, K.,
Kanakidou, M., Olgun, N., Peters, F., Pulido-Villena, E., Tovar-Sanchez, A., and
Völker, C.: The significance of episodicity in atmospheric deposition to Low Nutrient
1020 Low Chlorophyll regions, Global Biogeochem. Cycles, 28, 1179–1198,
doi:10.1002/2014GB004852, 2014a.

Guieu, C., Ridame, C., Pulido-Villena, E., Bressac, M., Desboeufs, K., and Dulac, F.: Impact
of dust deposition on carbon budget: a tentative assessment from a mesocosm approach,
Biogeosciences, 11, 5621-5635, doi: 10.5194/bg-11-5621-2014, 2014b.

1025 Guieu, C., D'Ortenzio, F., Dulac, F., Taillandier, V., Doglioli, A., Petrenko, A., Barrillon, S.,
Mallet, M., Nabat, P., and Desboeufs, K.: Process studies at the air-sea interface after
atmospheric deposition in the Mediterranean Sea: objectives and strategy of the
PEACETIME oceanographic campaign (May–June 2017), Biogeosciences, 17, 1–23,
2020, doi: 10.5194/bg-17-1-2020.

1030 Herut, B., Zohary, T., Krom, M.D., Mantoura, RFC., Pitta, P., Psarra, S., Rassoulzadegan, F.,
Tanaka, T. and Thingstad, T.F.: Response of East Mediterranean surface water to
Saharan dust:On-board microcosm experiment and field observations, Deep-Sea
Research II 52 (2005) 3024–3040, 2005.

Herut, B., Rahav, E., Tsagarakis, T. M., Giannakourou, A., Tsiola, A., Psarra, S., Lagaria, A.,
1035 Papageorgiou, N., Mihalopoulos, N., Theodosi, C. N., Violaki, K., Stathopoulou, E.,
Scoullos, M., Krom, M. D., Stockdale, A., Shi, Z., Berman-Frank, I., Meador, T. B.,
Tanaka, T., and Paraskevi, P.: The potential impact of Saharan dust and polluted
aerosols on microbial populations in the East Mediterranean Sea, an overview of a
mesocosm experimental approach, Front. Mar. Sci, 3, 226, doi:
1040 10.3389/fmars.2016.00226, 2016.

Holmes, R. M., Aminot, A., Kérouel, R., Hooker, B. A., and Peterson, B. J.: A simple and
precise method for measuring ammonium in marine and freshwater ecosystems, Can.
J. Fish. Aquat. Sci., 56, 1801-1808, 1999.



1045 Hoppe, H.-G., Ducklow, H., and Karrasch, B.: Evidence for dependency of bacterial growth on enzymatic hydrolysis of particulate organic matter in the mesopelagic ocean, *Mar. Ecol. Prog. Ser.*, 93, 277-283, 1993.

Ibello, V., Cantoni, C., Cozzi, S., and Civitarese, G.: First basin-wide experimental results on N₂ fixation in the open Mediterranean Sea, *Geophys. Res. Lett.*, 37, L03608, doi:10.1029/2009GL041635, 2010.

1050 Izquierdo, R., Benítez-Nelson, C. R., Masqué, P., Castillo, S., Alastuey, A., and Ávila, A.: Atmospheric phosphorus deposition in a near-coastal rural site in the NE Iberian Peninsula and its role in marine productivity, *Atmos. Environ.*, 49, 361–370, doi: 10.1016/j.atmosenv.2011.11.007, 2012.

Jumars, P. A., Penry, D. L., Baross, J. A., Perry, M. A., and Frost, B. W.: Closing the microbial loop : dissolved carbon pathway to heterotrophic bacteria from incomplete ingestion, digestion and absorption in animals, *Deep-Sea Research*, 483-495, 1989.

Kamykowski, D., and Zentara, S.J.: Nitrate and silicic acid in the world ocean: Patterns and processes, *Mar. Ecol. Prog. Ser.*, 26, 47–59, 1985

1055 Kanakidou, M., Myriokefalitakis, S., and Tsagaridis, K.: Aerosols in atmospheric chemistry and biogeochemical cycles of nutrients, *Environ. Res. Lett.*, 13, 063004, doi: 10.1088/1748-9326/aabedb, 2018.

Kanakidou, M., Myriokefalitakis, S., and Tsagkaraki, M.: Atmospheric inputs of nutrients to the Mediterranean Sea, *Deep Sea Research Part II: Topical Studies in Oceanography*, 171, 104606, doi: 10.1016/j.dsr2.2019.06.014, 2020.

1065 Kirchman, D. L. : Leucine incorporation as a measure of biomass production by heterotrophic bacteria. In: *Handbook of methods in aquatic microbial ecology*, edited by : Kemp, P.F., Sherr, B.F., Sherr, E.B. and Cole, J.J., Lewis, Boca Raton, 509-512, 1993.

Kouvarakis, G., Mihalopoulos, N., Tselepidis, T., and Stavrakakis, S.: On the importance of atmospheric nitrogen inputs on the productivity of eastern Mediterranean, *Global Biogeochemical Cycles*, 15, 805–818, doi:10.1029/2001GB001399, 2001.



Karl, D. M.: Microbially mediated transformations of phosphorus in the sea: New views of an old cycle. *Ann. Rev. Mar. Sci.* 6: 279–337, doi: 10.1146/annurev-marine-010213-135046, 2014.

1075 Krom, M. D., Herut, B., and Mantoura, R. F. C.: Nutrient budget for the eastern Mediterranean: Implication for phosphorus limitation, *Limnol. Oceanogr.* 49, 1582-1592, doi: 10.4319/lo.2004.49.5.1582, 2004.

Krom, M. D., Emeis, K.-C., and Van Capellen, P.: Why is the eastern Mediterranean phosphorus limited? *Progress In Oceanography*, 85, 236-244, 2010.

1080 Lindroth, P., and Mopper, K.: High performance liquid chromatographic determination of sub picomole amounts of amino acids by precolumn fluorescence derivatization with o-phthaldialdehyde, *Anal. Chem.* 51, 1667–1674, 1979.

Louis, J., Bressac, M., Pedrotti, M.-L., and Guiieu, C.: Dissolved inorganic nitrogen and phosphorus dynamics in sea water following an artificial Saharan dust deposition event, *Frontiers Marine Sci.*, 2, article 27, doi: 10.3389/fmars.2015.00027, 2015.

1085 Løvdal, T., Skjoldal, E. F., Heldal, M., Norland, S., and Thingstad, T. F.: Changes in Morphology and Elemental Composition of *Vibrio splendidus* Along a Gradient from Carbon-limited to Phosphate-limited Growth, *Microb. Ecol.*, 55, 152-161, doi: 10.1007/s00248-007-9262-x, 2008.

1090 Makino, W., Cotner, J. B., Sterner, R. W., and Elser, J. J.: Are bacteria more like plants or animals? Growth rate and resource dependence of bacterial C : N : P stoichiometry, *Functional Ecology*, 17, 121-130, 2003.

Malits, A., Cattaneo, R., Sintes, E., Gasol, J. M., Herndl, G. J., and Weinbauer, M.: Potential impacts of black carbon on the marine microbial community, *Aquat Microb Ecol.*, 75, 27-42, doi: 10.3354/ame01742, 2015.

1095 Marañón, E., Fernández, A., Mouríño-Carballido, B., Martínez-García, S., Teira, E., Cermeño, P., Chouciño, P., Huete-Ortega, M., Fernández, E., Calvo-Díaz, A., Morán, X. A. G., Bode, A., Moreno-Ostos, E., Varela, M. M., Patey, M. D., and Achterberg, E. P.: Degree of oligotrophy controls the response of microbial plankton to Saharan dust. *Limnology and Oceanography*, 55, 2339-2352, 2010



1100 Marañón, E., Van Wambeke, F., Uitz, J., Boss, E.S., Pérez-Lorenzo, M., Dinasquet, J.,
Haëntjens, N., Dimier, C., Taillardier, V.: Deep maxima of phytoplankton biomass,
primary production and bacterial production in the Mediterranean Sea during late
spring, *Biogeosciences Discuss.*, in review, bg 2020-261, 2020.

1105 Mari, X., Guinot, B., Chu, V. T., Brune, J., Lefebvre, J.-P., Pradeep Ram, A. S., Raimbault,
P., Dittmar, T., and Niggemann, J.: Biogeochemical Impacts of a Black Carbon Wet
Deposition Event in Halong Bay, Vietnam, *Front. Mar. Sci.*, 6, article 185, doi:
10.3389/fmars.2019.00185, 2019.

1110 Marie, D., Simon, N., Guillou, L., Partensky, F., and Vaulot, D.: Flow Cytometry Analysis of
Marine Picoplankton, in: *In Living Color: Protocols in Flow Cytometry and Cell*
Sorting, edited by: Diamond, R. A., and Demaggio, S., Springer, Berlin, Heidelberg,
421-454, 2000.

1115 Markaki, Z., Loyer-Pilot, M. D., Violaki, K., Benyahya, L., and Mihalopoulos, N.: Variability
of atmospheric deposition of dissolved nitrogen and phosphorus in the Mediterranean
and possible link to the anomalous seawater N/P ratio, *Marine Chemistry*, 120, 187-194,
doi: 10.1016/j.marchem.2008.10.005, 2010.

Martiny, A. C., Pham, C. T. A., Primeau, F. W., Vrugt, J. A., Moore, J. K., Levin, S. A., and
Lomas, M. W.: Strong latitudinal patterns in the elemental ratios of marine plankton and
organic matter, *Nature geosciences*, 6, 279-283, doi: 10.1038/ngeo1757, 2013

1120 Mermex Group.: Marine ecosystems' responses to climatic and anthropogenic forcings in the
Mediterranean, *Progress in Oceanography*, 91, 97-166, doi:
10.1016/j.pocean.2011.02.003, 2011.

Moreno, A.R., and Martiny, A.C.: Ecological stoichiometry of ocean plankton, *Ann. Rev. Mar. Sci.*, 10, 43-69, 2018.

1125 Moutin, T., and Prieur, L.: Influence of anticyclonic eddies on the Biogeochemistry from the
Oligotrophic to the Ultraoligotrophic Mediterranean (BOUM cruise). *Biogeosciences*, 9
(10), pp.3827 - 3855. 10.5194/bg-9-3827-2012, 2012.

Nagata, T.: Carbon and Nitrogen content of natural planktonic bacteria, *Appl., Environ. Microbiol.*, 52, 28-32, 1986.



1130 Orsini, D., Ma, Y., Sullivan, A., Sierau, B., Baumann, K., and Weber, R.: Refinements to the
Particle-Into-Liquid Sampler (PILS) for Ground and Airborne Measurements of Water
Soluble Aerosol Composition, *Atmospheric Environment*, 37, 1243-1259, 2003.

Omand, M. M. and Mahadevan, A.: The shape of the oceanic nitracline, *Biogeosciences*, 12,
3273–3287, doi: 10.5194/bg-12-3273-2015, 2015.

Pujo-Pay, M., and Raimbault, P.: Improvements of the wet-oxidation procedure for
1135 simultaneous determination of particulate organic nitrogen and phosphorus collected
on filters, *Mar. Ecol. Prog. Ser.*, 105, 203-207, 1994.

Pradeep Ram, A. S., and Sime-Ngando, T.: Resources drive trade-off between viral lifestyles
in the plankton: evidence from freshwater microbial microcosms, *Environ Microbiol*,
12, 467-479, doi: 10.1111/j.1462-2920.2009.02088.x, 2010.

1140 Pulido-Villena, E., Van Wambeke, F., Desboeufs, K., Petrenko, A., Barrillon, S., Djaoudi, K.,
Doglioli, A., D'Ortenzio, F., Fu, Y., Gaillard, T., Guasco, S., Nunige, S., Raimbault,
P., Taillandier, V., Triquet, S., and Guieu, C.: Phosphorus cycling in the upper waters
of the Mediterranean Sea (Peacetime cruise): relative contribution of external and
internal sources, this special issue, in preparation.

1145 Pulido-Villena, E., Wagener, T., and Guieu, C.: Bacterial response to dust pulses in the
western Mediterranean: Implications for carbon cycling in the oligotrophic ocean,
Global Biogeochem. Cy., 22, GB1020, doi:10.1029/2007GB003091, 2008.

Pulido-Villena, E., Baudoux, A.-C., Obernosterer, I., Landa, M., Caparros, J., Catala, P.,
1150 Georges, C., Harmand, J., and Guieu, C.: Microbial food web dynamics in response to
a Saharan dust event: results from a mesocosm study in the oligotrophic
Mediterranean Sea, *Biogeosciences*, 11, 337-371, 2014.

Rahav, E., Herut, B., Stambler, N., Bar-Zeev, E. Mulholland, M.R., and Berman-Frank, I.:
Uncoupling between dinitrogen fixation and primary productivity in the eastern
Mediterranean Sea, *J. Geophys. Res. Biogeosci.*, 118, 195–202,
1155 doi:10.1002/jgrg.20023, 2013a



Rahav, E. Herut, B., Levi, A., Mulholland, M.R., and Berman-Frank, I.: Springtime contribution of dinitrogen fixation to primary production across the Mediterranean Sea. *Ocean Sci.* 9, 489–498. doi: 10.5194/os-9-489-2013, 2013b.

1160 Rahav, E., Paytan, A., Chien, C.-T., Ovadia, G., Katz, T., and Herut, B.: The Impact of Atmospheric Dry Deposition Associated Microbes on the Southeastern Mediterranean Sea Surface Water following an Intense Dust Storm, *Front. Mar. Sci.* 3, 127, doi: 10.3389/fmars.2016.00127, 2016.

1165 Richon, C., Dutay, J. C., Dulac, F., Wang, R., Balkanski, Y., Nabat, P., Aumont, O., Desboeufs, K., Laurent, B., Guieu, C., Raimbault, P., and Beuvier, J.: Modeling the impacts of atmospheric deposition of nitrogen and desert dust-derived phosphorus on nutrients and biological budgets of the Mediterranean Sea, *Prog. Oceanogr.* 163, 21–39, doi: 10.1016/j.pocean.2017.04.009, 2018.

1170 Ridame, C., Moutin, T. and C. Guieu.: Does phosphate adsorption onto Saharan dust explain the unusual N/P ratio in the Mediterranean Sea ? *Oceanologica Acta*, 26, 629-634, doi: 10.1016/S0399-1784(03)00061-6, 2003.

Ridame C., M. Le Moal, C. Guieu, E. Ternon, I. C. Biegala, S. L'Helguen, and M. Pujo-Pay.: Nutrient control of N₂ fixation in the oligotrophic Mediterranean Sea and the impact of Saharan dust events, *Biogeosciences*, 8, 2773-2783, doi:10.5194/bg-8-2773-2011, 2011.

1175 Ridame C., Dinasquet J., Bigeard E., Hallstrom, S., Riemann L., Tovar-Sanchez A., Gazeau F. Baudoux A-C., Guieu C., Impact of dust enrichment on N2 fixation and diversity of diazotrophs under present and future conditions of pH and temperature, this special issue, in preparation.

1180 Sala, M. M., Peters, F., Gasol, J. M., Pedros-Alio, C., Marrasse, C., and Vaque, D.: Seasonal and spatial variations in the nutrient limitation of bacterioplankton growth in the northwestern Mediterranean, *Aquat. Microb. Ecol.*, 27, 47-56, 2002.

Sandroni, V., Raimbault, P., Migon, C., Garcia, N., and Gouze, E.: Dry atmospheric deposition and diazotrophy as sources of new nitrogen to northwestern Mediterranean oligotrophic surface waters, *Deep-Sea Res. I*, 54, 1859–1870, doi:10.1016/j.dsr.2007.08.004, 2007.



1185 Taillandier, V., Prieur, L., D'Ortenzio, F., Ribera d'Alcalà, M., and Pulido-Villena, E.:
Profiling float observation of thermohaline staircases in the western Mediterranean Sea
and impact on nutrient fluxes, *Biogeosciences*, 17, 3343–3366, 2020.

1190 Talarmin A, Van Wambeke F., Lebaron P., and Moutin T.: Vertical partitioning of phosphate
uptake among picoplankton groups in the low Pi Mediterranean Sea, *Biogeosciences*,
12: 1237-1247 doi:10.5194/bg-12-1237-2015, 2015.

1195 Tanaka, T., Thingstad, T. F., Christaki, U., Colombet, J., Cornet-Barthaux, V., Courties, C.,
Grattepanche, J.-D., Lagaria, A., Nedoma, J., Oriol, L., Psarra, S., Pujo-Pay, M., and
Van Wambeke, F.: Lack of P-limitation of phytoplankton and heterotrophic prokaryotes
in surface waters of three anticyclonic eddies in the stratified Mediterranean Sea,
Biogeosciences, 8, 525, doi: 10.5194/bg-8-525-2011, 2011.

Thingstad, T. F., and Rassoulzadegan, F.: Nutrient limitations, microbial food webs, and
'biological C-pumps': suggested interactions in a P-limited Mediterranean, *Mar. Ecol. Prog. Ser.*, 117, 299-306, 1995.

1200 Thingstad, T., Krom, M. D., Mantoura, F., Flaten, G., Groom, S., Herut, B., Kress, N., Law,
C. S., Pasternak, A., Pitta, P., Psarra, S., Rassoulzadegan, F., Tanaka, T., Tselepides, A.,
Wassmann, P., Woodward, M., Riser, C., Zodiatis, G., and Zohary, T.: Nature of
phosphorus limitation in the ultraoligotrophic eastern Mediterranean, *Science*, 309,
1068-1071, doi: 10.1126/science.1112632, 2005.

1205 Van Wambeke, F., Christaki, U., Giannakourou, A., Moutin, T., and Souvmerzoglou, K.:
Longitudinal and vertical trends of bacterial limitation by phosphorus and carbon in
the Mediterranean Sea, *Microb. Ecol.*, 43, 119-133, doi: 10.1007/s00248-001-0038-4,
2002.

1210 Van Wambeke, F., Gimenez, A., Duhamel, S., Dupouy, C., Lefevre, D., Pujo-Pay, M., and
Moutin, T.: Dynamics and controls of heterotrophic prokaryotic production in the
western tropical South Pacific Ocean: links with diazotrophic and photosynthetic
activity, *Biogeosciences*, 15: 2669 – 2689, doi: 10.5194/bg-15-2669-2018, 2018.

Van Wambeke, F., Pulido-Villena, E., Dinasquet, J., Djaoudi, K., Engel, A., Garel, M.,
Gusaco, S., Nunige, S., Taillandier, V., Zäncker, B., and Tamburini, C.: Spatial



1215 patterns of biphasic ectoenzymatic kinetics related to biogeochemical properties in the
Mediterranean Sea, Biogeosciences Discuss., in review, bg-2020-253, 2020.

1220 Vincent, J., Laurent, B., Losno, R., Bon Nguyen, E., Roullet, P., Sauvage, S., Chevaillier, S.,
Coddeville, P., Ouboulmane, N., di Sarra, A. G., Tovar-Sánchez, A., Sferlazzo, D.,
Massanet, A., Triquet, S., Morales Baquero, R., Fornier, M., Coursier, C., Desboeufs,
K., Dulac, F., and Bergametti, G.: Variability of mineral dust deposition in the western
Mediterranean basin and south-east of France, *Atmos. Chem. Phys.*, 16, 8749–8766,
doi: 10.5194/acp-16-8749-2016, 2016.

Yelton, A.P., Acinas, S.G., Sunagawa, S., Bork, P., Pedros-Alio, C., Chisholm, S.W.: Global
genetic capacity for mixotrophy in marine picocyanobacteria. *ISME J* 10:2946-2957,
2016.

1225 Zhang, J.-Z., and Chi, J. : Automated analysis of nano-molar concentrations of phosphate in
natural waters with liquid waveguide, *Environ. Sci. Technol.*, 36, 1048-1053, doi :
10.1021/es011094v, 2002.



Table 1. Main biogeochemical features/trophic conditions during the PEACETIME cruise.

1230 For TYR, ION and FAST sites investigated during several days, means \pm sd are indicated.
 TChla: Integrated total chlorophyll a (Chla + dvChla). IPP: Integrated particulate primary production; IBP: integrated heterotrophic prokaryotic production from surface to 200 m depth.

	sampling date	Lat. °N	Long. °E	Temp. at 5 m °C	Bottom depth m	DCM depth m	TChl a mg chla m ⁻²	IPP mg C m ⁻² d ⁻¹	IBP mg C m ⁻² d ⁻¹
ST1	May 12	41°53.5	6°20	15.7	1580	49	35,0	284	51
ST2	May 13	40°30.36	6°43.78	17.0	2830	65	32,7	148	55
ST3	May 14	39°0.8.0	7°41.0	14.3	1404	83	23,2	140	77
ST4	May 15	37°59.0	7°58.6	19.0	2770	64	29,2	182	66
ST5	May 16	38°57.2	11°1.4	19.5	2366	77	30,5	148	51
TYR	May 17-20	39°20.4	12°35.56	19.6	3395	80 \pm 6	29 \pm 3	170 \pm 35	57 \pm 3
ST6	May 22	38°48.47	14°29.97	20.0	2275	80	18,7	142	62
ST7	May 24	36°39.5	18°09.3	20.6	3627	87	24.2	158	57
ION	May 25-28	35°29.1	19°47.77	20.6	3054	97 \pm 5	29 \pm 2	208 \pm 15	51 \pm 9
ST8	May 30	36°12.6	16°37.5	20.8	3314	94	31.6	206	71
ST9	June 2	38°08.1	5°50.5	21.2	2837	91	36.1	214	64
FAST	June 2-7 and 9	37°56.8	2°54.6	21.0	2775	79 \pm 8	34 \pm 8	211 \pm 57	92 \pm 11
ST10	June 8	37°27.58	1°34.0	21.6	2770	89	28,9	nd	96

1235



1240 **Table 2.** N budget at the short stations within the surface mixed layer (ML). Integrated stocks (NO₃, $\mu\text{mol N m}^{-2}$) and fluxes (heterotrophic prokaryotic N demand (hprokN demand), phytoplankton N demand (phytoN demand), in situ leucine aminopeptidase hydrolysis fluxes (LAP), dry atmospheric deposition of NO₃ and NH₄ (all fluxes in $\mu\text{mol N m}^{-2} \text{d}^{-1}$). Values presented as mean \pm sd. SD was calculated using propagation of errors of measurements (all data), C/N ratio of 7.3 ± 1.6 (hprokN demand) and 7 ± 1.4 (phytoN demand). MLD: mixed layer depth. na: not available because under LWCC detection limits.

stations	MLD	stocks	biological fluxes				Dry deposition	
			phytoN demand	hprokN demand	LAP	N ₂ fixation	NO ₃	NH ₄
	m	$\mu\text{mol N m}^{-2}$	$\mu\text{mol N m}^{-2} \text{d}^{-1}$					
ST1	21	na	1468 \pm 325	184 \pm 40	121 \pm 28	14.6 \pm 1.5	18.6 \pm 1.4	1.5 \pm 0.3
ST2	21	na	481 \pm 161	163 \pm 35	48 \pm 24	10.7 \pm 1.1	23.7 \pm 2.2	4.1 \pm 0.9
ST3	11	na	282 \pm 82	126 \pm 28	40 \pm 17	7.8 \pm 0.8	33.8 \pm 3.6	4.7 \pm 0.5
ST4	15	na	246 \pm 80	132 \pm 28	83 \pm 20	10.7 \pm 1.1	23.8 \pm 2.9	6.3 \pm 2.6
ST5	9	261 \pm 22	112 \pm 29	42 \pm 9	17 \pm 12	4.8 \pm 0.5	27.0 \pm 7.5	7.9 \pm 1.8
ST6	18	162 \pm 14	410 \pm 116	204 \pm 44	48 \pm 24	9.1 \pm 0.9	15.0 \pm 0.6	9.3 \pm 0.7
ST7	18	162 \pm 14	226 \pm 123	148 \pm 33	83 \pm 18	10.5 \pm 1.1	23.6 \pm 1.9	8.0 \pm 1.2
ST8	14	911 \pm 77	274 \pm 66	130 \pm 33	25 \pm 8	4.3 \pm 0.5	13.4 \pm 1.7	3.8 \pm 0.6
ST9	7	819 \pm 70	259 \pm 70	85 \pm 22	21 \pm 6	3.4 \pm 0.4	27.4 \pm 3.8	13.5 \pm 0.8
ST10	19	2074 \pm 176	495 \pm 31	294 \pm 64	42 \pm 26	13.6 \pm 1.4	23.9 \pm 3.4	4.1 \pm 0.4

1245



Table 3. Characteristics of the 2 rains collected during the PEACETIME cruise. The collector surface was 0.045 m²

event	Rain 1	Rain 2
Location	ION	FAST
Date and local time	29/05 05:08-6:00	05/06 02:36-3:04
Duration min	52	28
Collected volume ml	118	87.9
DIP Flux nmol P m ⁻²	495.5	129
DOP Flux nmol P m ⁻²	728.2	103
POP fluxes nmol P m ⁻²	179	994
NO ₃ Flux μmol N m ⁻²	50.0	115.7
NH ₄ Flux μmol N m ⁻²	53.2	70.6
DIN Flux μmol N m ⁻²	103	187

1250



Figure legends

Figure 1. Nitrate (NO_3) aerosol concentration along the PEACETIME transect. The location of two rain events are indicated by large black circles. Stations ST 1 to 4 were not sampled for analysis of nutrients at nanomolar level.

1255 **Figure 2.** Representation of the mixed layer (ML), the bottom of the nitrate (NO_3) depleted layer (NDLb), delineated by the nitracline depth and the mixed layer depth (MLD).

1260 **Figure 3.** a) Evolution of the wind speed during the cruise PEACETIME. The stations are indicated in yellow and dates in black. Vertical dotted lines delineate the beginning and the end of occupation of the ship at TYR, ION and FAST sites. The two rain events collected on board are indicated in solid vertical red arrows and surrounding observed rains by horizontal dashed red arrows. b) 0-100 m vertical distribution of nitrate (NO_3) with depth. The MLD (in red) and nitracline (in brown) are indicated.

1265 **Figure 4.** Average concentration of nitrate (NO_3) in the ML and the NDLb, and NO_3 flux from ML to NDLb. The stations have been classified into 4 types (1 in blue, 2 in green, 3 in yellow, 4 in red, see section Results and Table S1 for definitions). Error bars are indicated by standard deviation around average values for nitrate concentrations, and error propagation for the flux from ML to NDLb using a 0.5 m uncertainty in the MLD variation.

1270 **Figure 5.** Evolution within the ML of heterotrophic prokaryotic production (BP), particulate primary production (PP), heterotrophic prokaryotes (hprok) and *Synechococcus* (syn) abundances at the station FAST. The mixed layer depth is indicated in red line.

1275 **Figure 6.** Results of the enrichment experiment. BP reached after 36 h of enrichment in the dark. C: control unamended, P:+DIP, N:+ NO_3 + NH_4 , G:+glucose, and combinations of these elements in PN, NG, PG and NPG. Stars show significantly different BP compared to the unamended control .

Figure 7. Synthetic view of biogeochemical processes and exchanges between ML and NDLb before the rain and evolution after the rain.

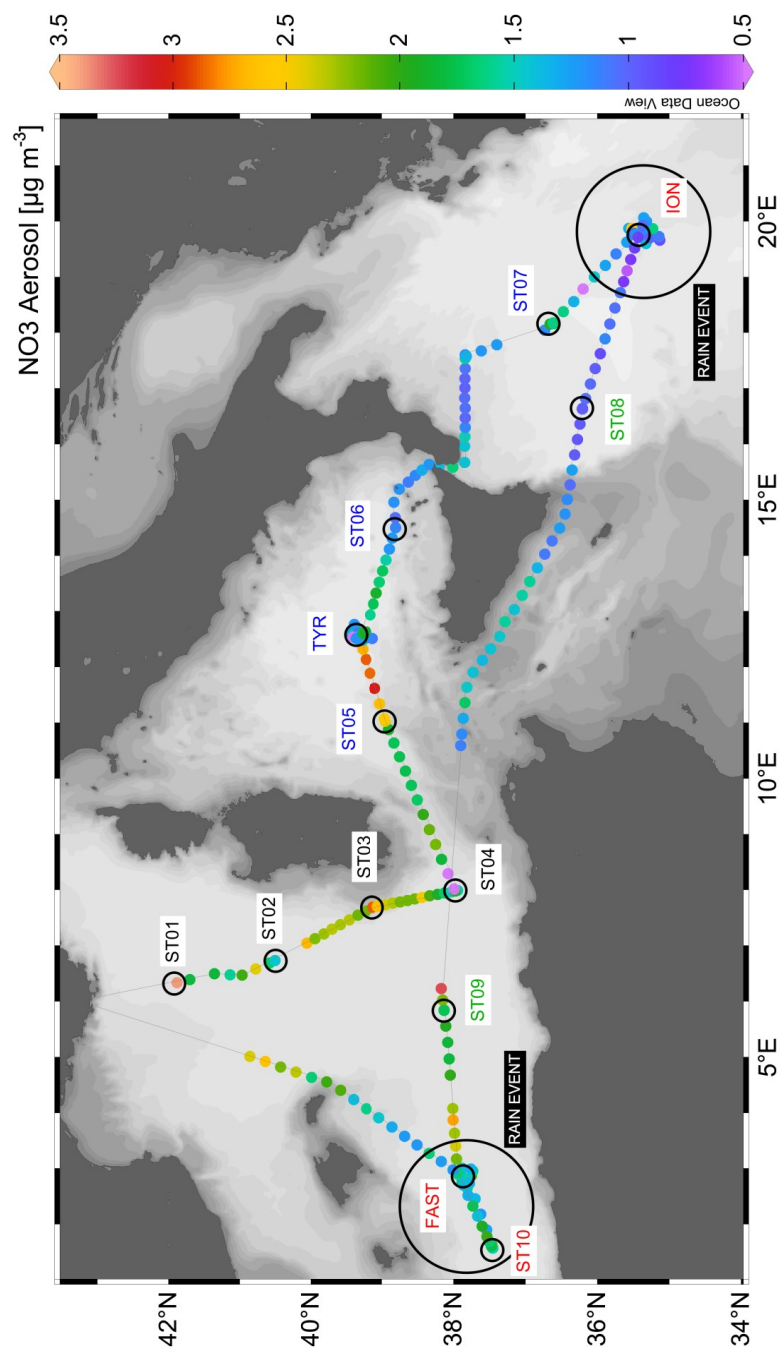


Fig. 1



Fig. 2

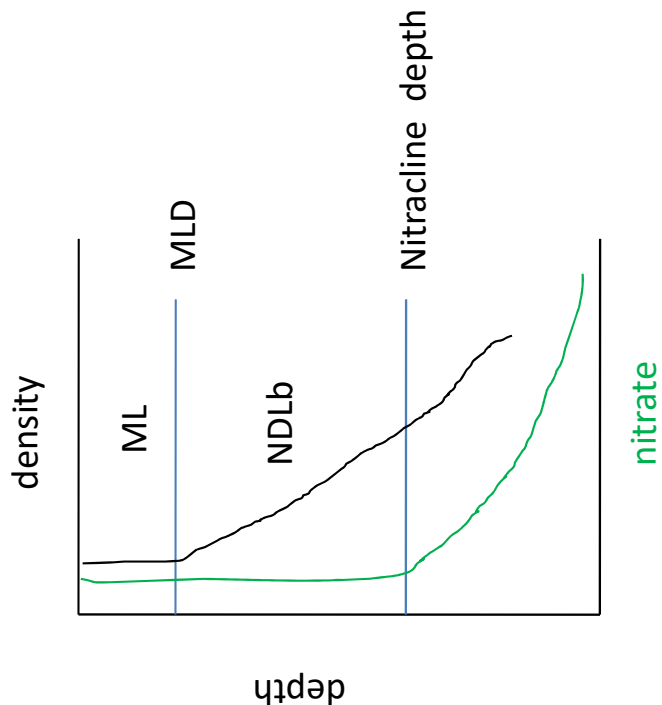




Fig. 3

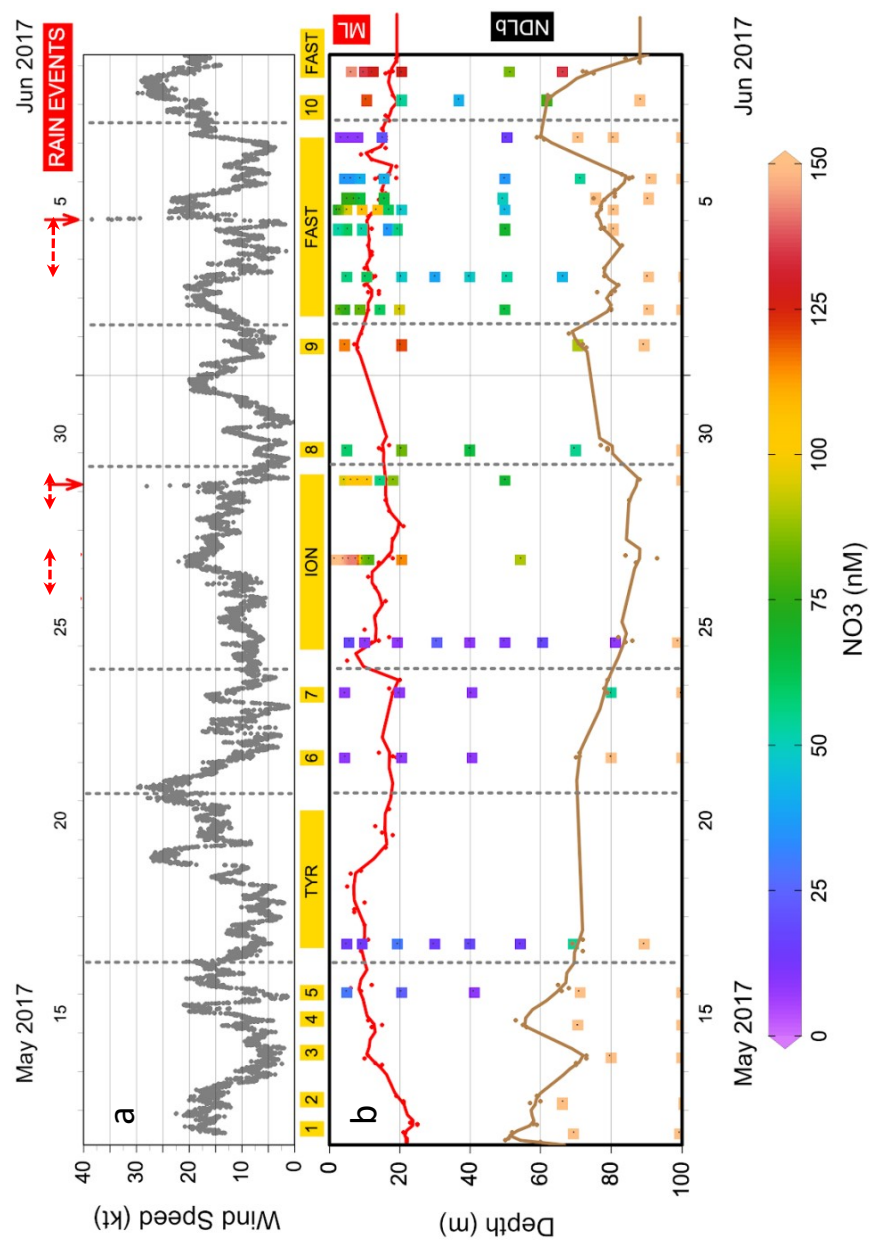
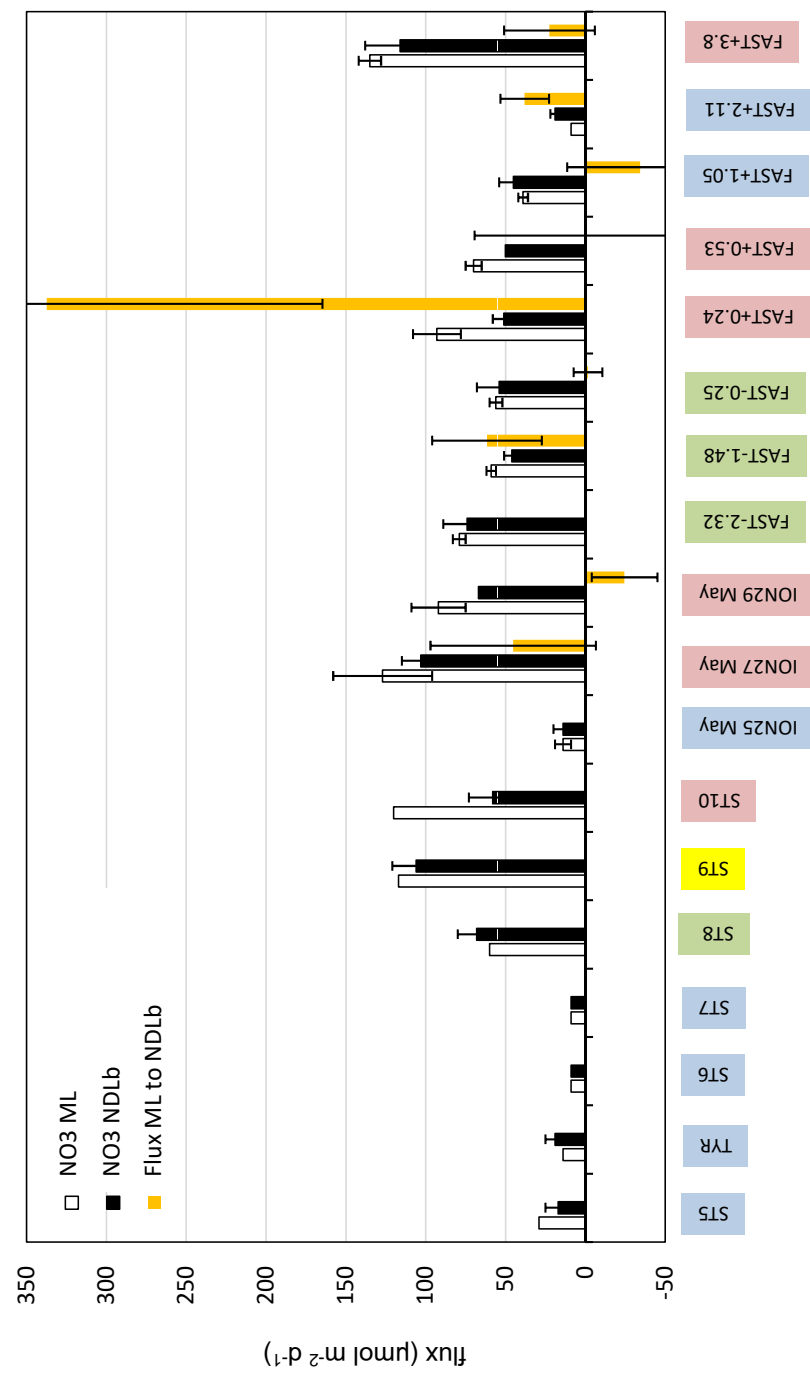




Fig. 4



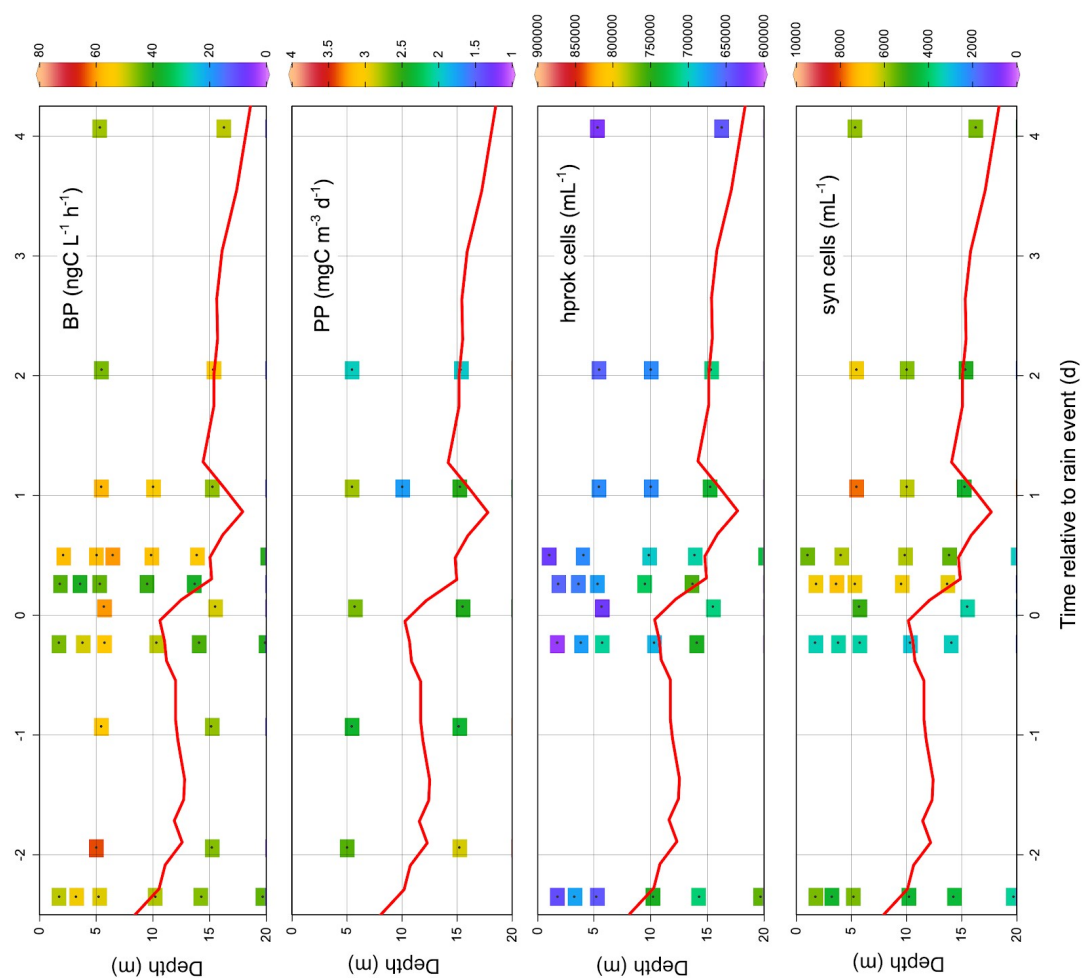


Fig. 5

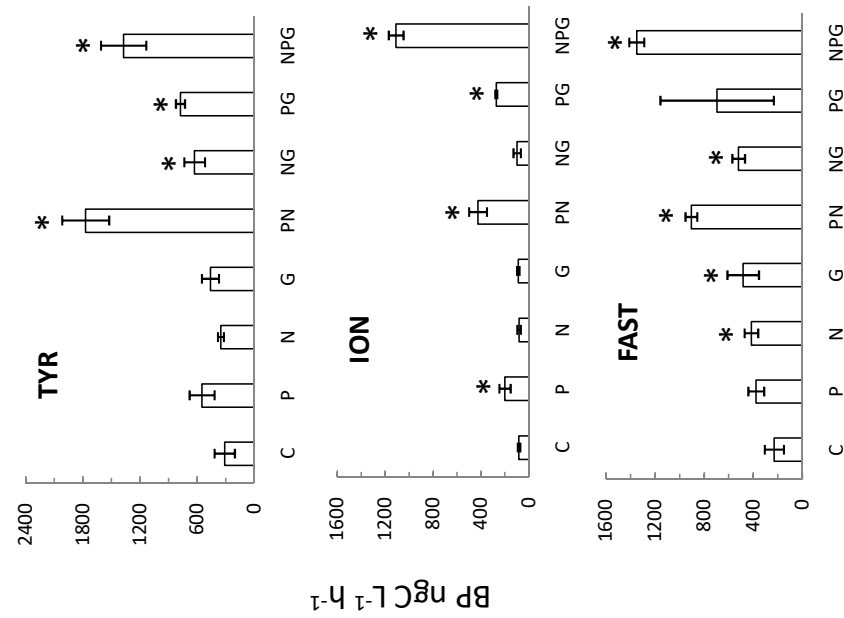


Fig. 6



Fig. 7

